AD/A-004 800

DESIGN OF A DEPLOYABLE WING GLIDER

Phillip L. Abold

Air Force Institute of Technology
Wright-Patterson Air Force Base, Ohio

December 1974

UNCLASSIFIED
SECURITY CLASSIFICATION OF THIS PAGE (When Data Entered)

REPORT DOCUMENTATION PAGE		READ INSTRUCTIONS BEFORE COMPLETING FORM
1. REPORT NUMBER GAE/MC/74D-1	2. GOVT ACCESSION NO.	3. RECIPIENT'S CATALOG NUMBER ADA-004800
4. TITLE (and Subtitle) DESIGN OF A DEPLOYABLE WING GLIDER		5. TYPE OF REPORT & PERIOD COVERED MS THESIS 6. PERFORMING ORG. REPORT NUMBER
7. AUTHOR(s) Phillip L. Abold Captain, USAF		8. CONTRACT OR GRANT NUMBER(s)
9. PERFORMING ORGANIZATION NAME AND ADDRESS Air Force Institute of Technology (AFIT-EN) Wright-Patterson AFB, Ohio 45433		10. PROGRAM ELEMENT, PROJECT, TASK AREA & WORK UNIT NUMBERS
11. CONTROLLING OFFICE NAME AND ADDRESS Air Force Flight Dynamics Laboratory Wright-Patterson AFB, Ohio 45433		12. REPORT DATE December 1974 13. NUMBER OF PAGES 76
14. MONITORING AGENCY NAME & ADDRESS(if different from Controlling Office)		15. SECURITY CLASS. (of this report) UNCLASSIFIED 15a. DECLASSIFICATION/DOWNGRADING SCHEDULE

16. DISTRIBUTION STATEMENT (of this Report)

Approved for public release; distribution unlimited

17. DISTRIBUTION STATEMENT (of the abstract entered in Block 20, if different from Report)

18. SUPPLEMENTARY NOTES

Approved for public release
IAW AFR 190-17

JERRY C. HIX, Captain, USAF
Director of Information

19. KEY WORDS (Continue on reverse side if necessary and identify by block number)

unguided glider
electronic countermeasures

20. ABSTRACT (Continue on reverse side if necessary and identify by block number)

An unpowered, unguided vehicle to be deployed from a 4.75" flare tube was designed. The design criteria were:

1) six cubic inch, two pound payload
2) minimum glide speed of 50 knots
3) stable with particular emphasis on heading stability.

Two basic configurations were considered in the analysis: the first was a tailless vehicle, and the second was a conventionally tailled vehicle. It was found that the tailless vehicle could not meet the stability requirements

DD FORM 1 JAN 73 1473 EDITION OF 1 NOV 65 IS OBSOLETE

UNCLASSIFIED
SECURITY CLASSIFICATION OF THIS PAGE (When Data Entered)

Block 20

and thus the tailled vehicle was chosen to meet the design criteria. The analysis procedure consisted of a computer model to analyze vehicle stability, wind tunnel tests to calculate aerodynamic derivatives, and flight tests to demonstrate performance. The finalized vehicle had a folding wing and flexible tail-boom to meet the packaging requirement. The resulting vehicle had a glide ratio of 25 and was very stable in heading, while meeting all other design requirements.

GAE/MC/74D-1

DESIGN OF A DEPLOYABLE WING GLIDER

THESIS

Presented to the Faculty of the School of Engineering of the

Air Force Institute of Technology

Air University

in Partial Fulfillment of the

Requirements for the Degree of

Master of Science

by

Phillip L. Abold, B.S.A.E.

Captain USAF

Graduate Aeronautical Engineering

December 1974

ii

Preface

Despite very rapid developments in aerodynamic theory and the great improvements in the useage of this theory through the development of modern computer facilities, much of the design work on unusual configurations is a trial and error process that utilizes approximate mathematical models of the configuration to aid the designer in the analysis of these configurations. The following thesis demonstrates the application of this design process to a specific design request from the Air Force Avionics Laboratory. The trial and error process would have been more error than trial were it not for the help of Mr. Russel Osborne, an engineer for the Air Force Flight Dynamics Laboratory. I would also like to thank my thesis advisor for his patience and for providing some necessary direction. Additional thanks go to the Air Force Institute of Technology Model Shop for their patience in building and frequently repairing the test models necessary for this investigation. It goes without saying that I owe much to my wife, Scotty, for insulating me from the outside world while writing this report.

Phillip L. Ahold

Contents

List of Figures

Notation

A_N	Fourier coefficient
b	Wing span
b_H	Horizontal stabilizer span
b_v	Vertical stabilizer span
C_{D_e}	Vehicle equilibrium drag coefficient
C_{D_α}	Vehicle drag change with angle of attack
C_{L_e}	Vehicle equilibrium lift coefficient
C_{L_q}	Change in lift with pitch rate
C_{L_α}	Vehicle lift change with angle of attack
$C_{L_{\dot\alpha}}$	Change in lift with angle of attack rate
$C_{l_{\alpha_H}}$	Horizontal stabilizer lift change with angle of attack
$C_{l_{\alpha_W}}$	Wing lift change with angle of attack
C_{l_β}	Change in rolling moment with sideslip
C_{l_p}	Change in rolling moment with roll rate
C_{l_r}	Change in rolling moment with yaw rate
C_M	Vehicle coefficient of moment
C_{M_o}	Zero lift coefficient of moment
C_{M_q}	Change in moment with pitch rate
C_{M_α}	Change in moment with angle of attack
$C_{M_{\dot\alpha}}$	Change in moment with angle of attack rate
C_{n_β}	Change in yawing moment with sideslip
C_{n_p}	Change in yawing moment with roll rate
C_{n_r}	Change in yawing moment with yaw rate
C_{Y_β}	Change in sideforce with sideslip

$C_{y_{\beta_v}}$	Change in sideforce with sideslip due to vertical stabilizer
C_{y_p}	Change in sideforce with roll rate
C_{y_r}	Change in side force with yaw rate
C_{w_e}	Equilibrium weight coefficient
c	Wing chord
c_H	Horizontal stabilizer chord
c_v	Vertical stabilizer chord
g	Acceleration of gravity
$\hat{I}'_x$	Nondimensional rolling moment of inertia
$\hat{I}'_y$	Nondimentional pitching moment of inertia
$\hat{I}'_z$	Nondimentional yawing moment of inertia
k_n	Static margin
l_b	Body horizontal length
l_v	Length from vehicle center of gravity to horizontal stabilizer aerodynamic center
S	Wing Area
S_H	Horizontal stabilizer area
S_o	Body cross-sectional area at point of maximum thickness
S_v	Vertical stabilizer area
T	Oscillation period
$\overline{V}_H$	Tail volume coefficient
w	Vehicle weight
z_v	Vertical distance from vehicle center of gravity to aerodynamic center of vertical stabilizer
AR	Aspect ratio
Γ	Wing dihedral
γ_e	Flight path angle
ζ	Damping coefficient

Abstract

An unpowered, unguided vehicle to be deployed from a 4.75" flare tube was designed. The design criteria were:

1) six cubic inch, two pound payload
2) minimum glide speed of 50 knots
3) glide ratio in excess of five
4) stable with particular emphasis on heading stability

Two basic configurations were considered in the analysis: the first was a tailless vehicle, and the second was a conventionally tailed vehicle. It was found that the tailless vehicle could not meet the stability requirements and thus the tailed vehicle was chosen to meet the design criteria. The analysis procedure consisted of a computer model to analyze vehicle stability, wind tunnel tests to calculate aerodynamic derivatives, and flight tests to demonstrate performance. The finalized vehicle had a folding wing and a flexible tail-boom to meet the packaging requirement. The resulting vehicle had a glide ratio slightly in excess of 25 and was very stable in heading, while meeting all other design requirements.

DESIGN OF A DEPLOYABLE WING GLIDER

I. Introduction

The Problem

In an era of ever changing aerial tactics and countertactics, a constant search for new weapons is maintained. The design of one such weapon system is the subject of this thesis. The Air Force Avionics Laboratory requested the design of an unpowered, unguided, airborne vehicle capable of carrying a six cubic inch payload weighing two pounds at a minimum glide speed of 50 knots. To achieve maximum dispersal capability, each vehicle must maintain its deployment no-wind heading, and must be of minimum volume so that maximum numbers may be carried by the carrier vehicle. To eliminate the need for development and qualification of a new store, the proposal required that the vehicle be able to be carried in a 4.75 inch flare tube, thus presenting a significant packaging problem. In summary the problem presented was to design a vehicle subject to the following constraints:

1) unpowered and unguided
2) six cubic inch, two pound payload capacity
3) minimum glide speed of 50 knots
4) glide ratio in excess of five
5) stable with particular emphasis on heading stability
6) minimum size and packageable in a 4.75 inch tube.

The Analysis Procedure

As in any design study, the method used to create the final result was one of iteration among the best solutions to each of the design criteria. This analytic process used the most simple methods suitable to the complexity of the problem and testing methods utilizing the best available equipment. The procedure used in this design effort was divided into four parts: an extensive literature search to find the most suitable configuration for the required mission; the creation of a useable mathematical model to describe the chosen configuration; wind tunnel tests to determine the required aerodynamic coefficients; and flight tests of the various test vehicles.

Iteration among each of the latter three areas was accomplished to enable the chosen configurations to be optimized for the mission. This particular type of design process allowed the configuration to be modified during the process with little interruption of the test sequence.

Limitations and Assumptions

The design process did not include certain areas that would be of interest in further studies of the design. These areas include deployment aerodynamics and stability, and a structural analysis designed to determine the construction materials which provide the best compromise between weight, strength, and flexibility. These two areas were beyond the scope of this study due to limitations in the available facilities and time.

The major assumptions in the analytical modeling concerned linearity of the aerodynamics and of the equations of motion used in the stability analysis. Both of the assumptions are normally made in the preliminary

design phase, and are particularly valid for a glider designed to maintain a symmetrical equilibrium flight condition. The assumption of linear aerodynamics made the stability analysis possible since the stability derivatives were then possible to evaluate as functions of the planform and equilibrium flight condition. Further assumptions concerning each particular configuration will be discussed as they arise.

Order of Discussion

The report first discusses the choice of configurations to be considered, and then describes the entire analytic process for each of the chosen configurations. Although all of the phases for each configuration were carried out simultaneously, the description of the entire analysis procedure for one configuration at a time leads to a more understandable presentation. Specific conclusions concerning each configuration are presented at the end of the discussion of that particular configuration, while general conclusions and recommendations are presented at the end of the report.

II. THE CONFIGURATION

Configurations

The initial choice of configurations to be considered was important because it provided direction to the entire design process. It was possible to rapidly eliminate some configurations from further study because of their inherent limitations. In particular, both balloons and parachutes could not meet the requirement for a forward velocity of 50 knots and were therefore eliminated from consideration. All parafoil devices had to be eliminated due to glide ratios possible, although in every other respect they presented an excellent solution. It was possible that a hybrid vehicle, part balloon and part rigid wing, could have met the design requirements, but storage difficulties for such a vehicle eliminated it from consideration. As a result of the above eliminations, only rigid wing vehicles were studied further.

Three possible configurations were evaluated for possible study and two with their modifications were chosen to be studied. The three configurations studied were: an all-wing, a wing-body, and a conventional tailed vehicle.

The all-wing vehicle was first considered to represent the best possible solution to the overall problem. After studying possible planforms; however, it was found that an excessively large vehicle would be necessary to provide sufficient useable payload volume. Such a large vehicle presented a formidable packaging problem, and the folding mechanism was excessively complex. For these reasons, the all-wing design was not considered further.

The wing-body was considered to be the next best solution. This vehicle was more easily packaged than the all-wing vehicle, had the potential for higher performance than the conventional configuration due to lower expected drag, and provided a less complex folding problem than the conventional vehicle and was thus expected to be more reliable. The critical design point for this configuration was the stability requirement. This point was expected to present problems since a study of available literature, in particular reference 1, indicated that tailless vehicles were often only weakly stable, if stable at all, in some flight modes. If this design requirement could be met, then this configuration appeared to present the best solution to the design problem.

The least desirable configuration from preliminary estimates was the conventional vehicle. The design was the most complex mechanically and thus probably the most unreliable of the two possible configurations. It did have certain advantages; however, it presented the most stable configuration, and had the advantage of being better known so that the design process could be better analyzed.

Configuration Geometry

After the two basic configurations were decided upon, the basic planform parameters were obtained from an analysis of the packaging problem. The more complex packaging problem was the conventional vehicle and so it was chosen to determine the gross dimensions. To facilitate the construction and testing of the wind tunnel and flight test models, and to aid in the comparison of the two configurations, as much commonality as was possible was maintained between the vehicles. After many cut-and-try "paper doll" models, the final gross dimensions shown in figures 1 and 2 were chosen.

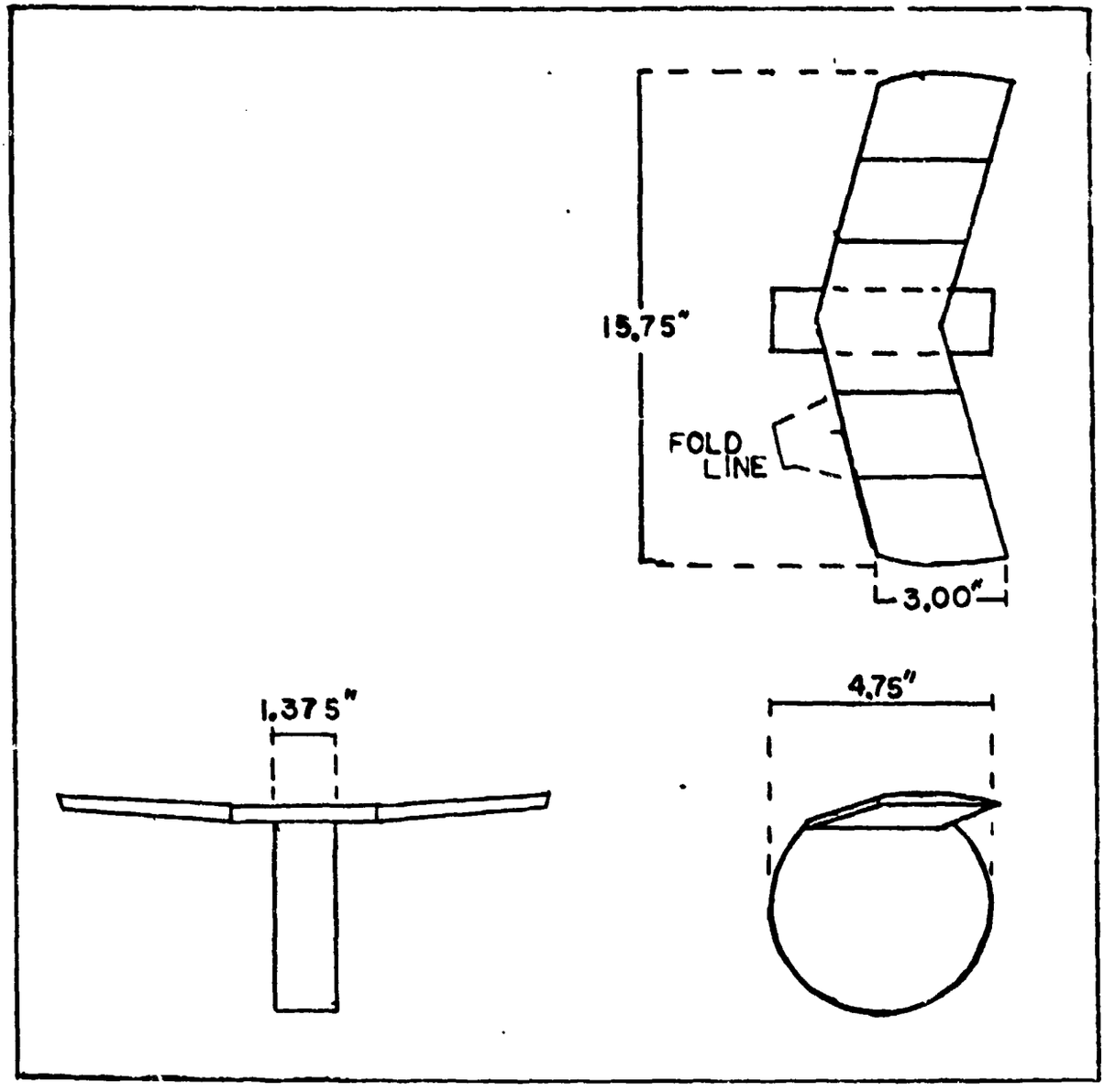

Fig. 1. Wing-Body Configuration

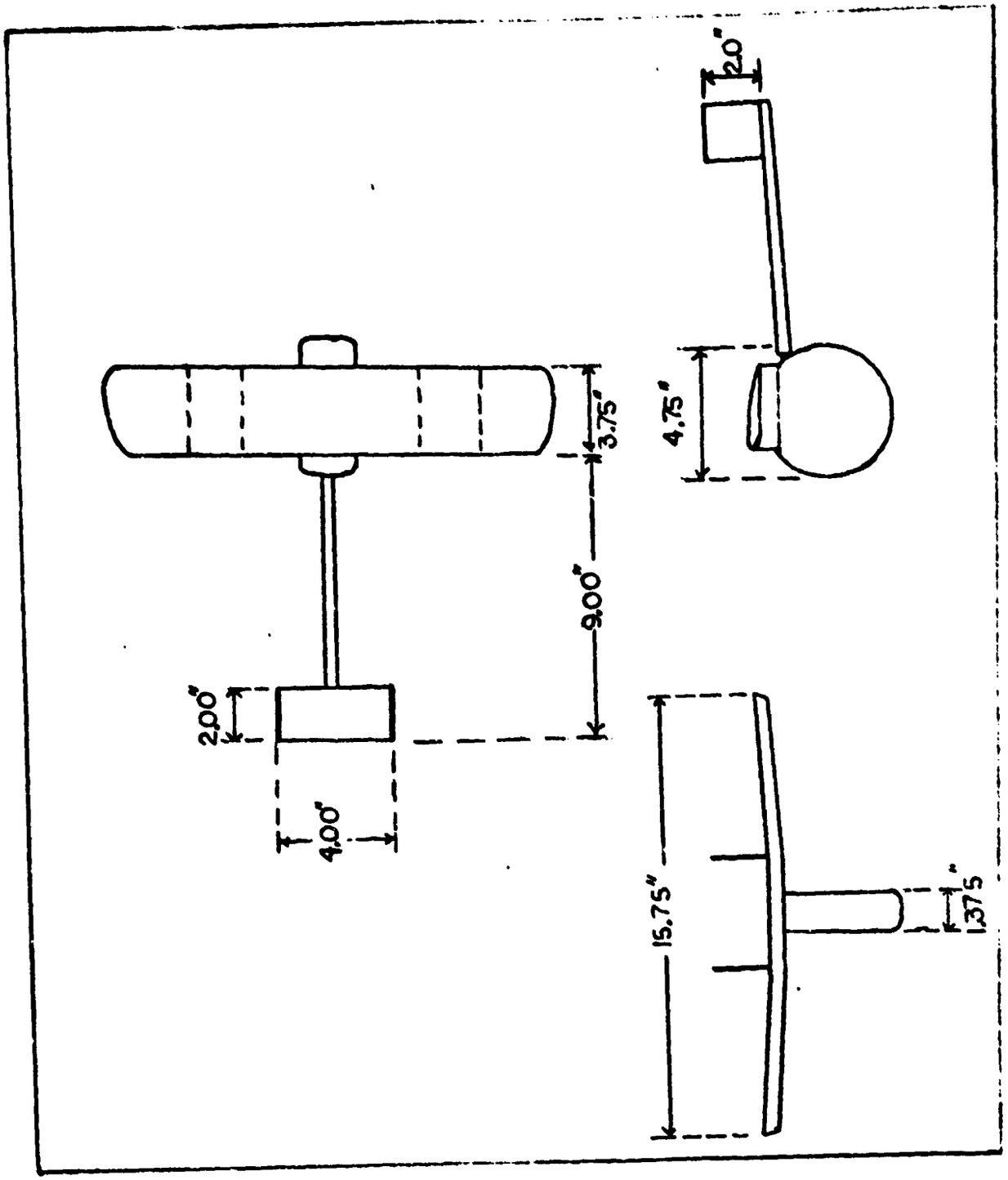

Fig. 2. Wing-Body-Tail Configuration

Although the chosen airfoil section, an NACA 4412, did not represent the optimum solution to the wing-body problem, it did present a ready solution to the folding problem as a result of its nearly flat bottom surface. A wing folding mechanism was designed for this wing by Mr. Lance Look of LOM Company under contract from the Air Force Flight Dynamics Laboratory. Through use of a simple tension spring system, the wing was folded at two points on each semi-span as shown in figures 1 and 2.

A low drag wing tip shape was developed using information from reference 2. The horizontal cross section of the body was chosen to be symmetrical with the point of maximum thickness located at the body midpoint. This profile was used rather than a more streamlined shape in an attempt to ensure that the body center of pressure was behind the center of gravity for the entire static margin range so that directional stability would not be a problem.

The one remaining parameter to be established was the wing sweep. In the conventional vehicle, a wing sweep angle of 0 degrees was chosen to provide maximum lift at lower angles of attack and thus to reduce the drag. In the wing-body, wing sweep was a necessity to ensure sufficient static margin range to provide longitudinal stability. Wing sweep moved the aerodynamic center aft and allowed greater latitude in payload location. After making the assumption that the wing aerodynamic center was at the .25 mean aerodynamic chord and that this chord was located at the area center of the semi-span, a good assumption in view of the method of reference 3 in locating this chord, it was found that a sweep angle of 15 degrees would provide a static margin range in excess of .30 while presenting the least possible compromise with performance.

III. THE WING-BODY DESIGN

Airfoil Design

All flight vehicles must satisfy the following three requirements to be able to achieve stable, trimmed flight: a positive C_{M_o}, a negative C_{M_α}, and a $C_M=0$ at some angle of attack greater than zero (Ref 4). In order to provide this capability, a modification of the basic NACA 4412 airfoil section had to be developed since a positively cambered airfoil could not provide the required positive C_{M_o} and no other airfoil section could be found to provide the required aerodynamic coefficients and meet the requirement that the bottom surface be flat for packaging purposes. Several solutions to this problem were available among which were utilizing geometric twist, upward deflected flaps, or a reflexed camber line. The simplest solutions were either flaps or a reflexed camber line since twist would require construction of a new wing, while the other solutions only meant sectioning the wing. The best solution from the packaging standpoint was the reflexed camber line so this solution was used.

One major assumption was made in the development of this wing; that creating an airfoil section with sufficient reflex would provide sufficient accuracy, ignoring all three dimensional effects, so that the actual wing camber line could be refined in the wind tunnel without reconstruction. Resulting wind tunnel tests proved the validity of this assumption.

The theory of thin wing sections used in the airfoil design (Ref 5) was iterated over several profiles until the desired properties were obtained. The necessary wing C_{l_1}, obtained from a summation of moments about the aerodynamic center assuming a static margin of .20 and neglecting drag effects on the moment balance, was .1450. This C_{l_1} yielded a vehicle $C_M=0$

at an arbitrary 10° angle of attack. Making the assumption that the airfoil could be represented as shown below in figure 3.

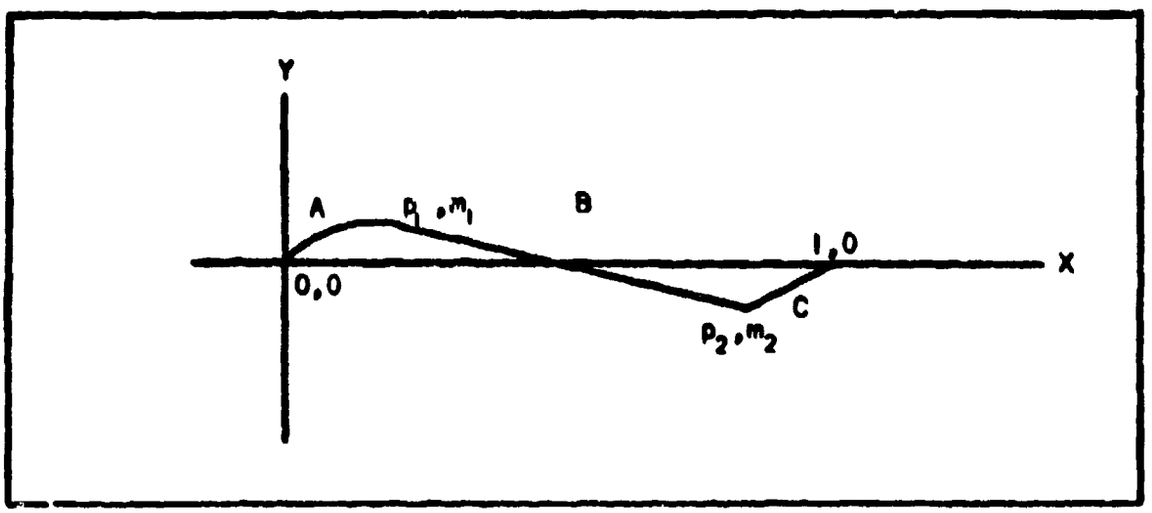

Fig. 3 Reflexed Camber Airfoil

and that line A was parabolic in shape, lines B and C were straight, the equations for each line were solved by matching boundary conditions at points (p_1, m_1) and (p_2, m_2). The slopes of the lines at these same points were obtained in gereral terms as:

$$\frac{dy}{dx_A} = \frac{(2x-p_1)(m_2p_1-m_1p_2) + m_1(p_1p_2-p_1^2)}{p_1^2(p_2-p_1)} \tag{1}$$

$$\frac{dy}{dx_B} = \frac{m_2-m_1}{p_2-p_1} \tag{2}$$

$$\frac{dy}{dx_C} = \frac{m_2}{p_2-1} \tag{3}$$

After utilizing Glauert's equation for the Fourier coefficients:

$$A_N = \frac{2}{\pi}\int_0^{\pi} \frac{dy}{dx} \cos n\theta \, d\theta \tag{4}$$

where: (5)

$$x = 1/2 (\cos \theta + 1)$$

the Fourier coefficients necessary to calculate C_l and C_m were:

$$A_0 = \frac{2}{\pi}\left[\frac{m_2}{p_2-1}\cos^{-1}(2p_2-1) + \frac{m_2-m_1}{p_2-p_1}(\cos^{-1}(2p_1-1) - \cos^{-1}(2p_2-1))\right.$$

$$+ \frac{(m_2p_1-m_1p_2)(1-p_1) + m_1(p_1p_2-p_1^2)}{p_1^2(p_2-p_1)}(\pi-\cos^{-1}(2p_1-1)) + \qquad (6)$$

$$\left. + \frac{m_2p_1-m_1p_2}{}(-\sin(\cos^{-1}(2p_1-1)))\right]$$

$$A_1 = \frac{2}{\pi}\left[\frac{m_2}{p_2-1}\sin(\cos^{-1}(2p_2-1)) + \frac{m_2m_1}{p_2p_1}(\sin(\cos^{-1}(2p_1-1))-\sin(\cos^{-1}(2p_2-1)))\right.$$

$$+ \frac{(1-p_1)(m_2p_1-m_1p_2) \quad m_1(p_2p_1-p_1^2)}{(p_1^2)(p_2-p_1)}(-\sin(\cos^{-1}(2p_1-1))) \qquad (7)$$

$$\left. + \frac{m_2p_1-m_1p_2}{p_1^2(p_2-p_1)}\left(\frac{\pi}{2} - \cos^{-1}(2p-1) + \frac{(\sin(\cos^{-1}(2p-1))))}{}\right)\right]$$

$$A_2 = \frac{2}{\pi}\left[\frac{m_2}{p_2-1}\frac{\sin(2\cos^{-1}(2p_2-1))}{2} + \frac{m_2-m_1}{p_2-p_1}\frac{(\sin(2\cos^{-1}(2p_1-1))-\sin(2\cos^{-1}(2p_2-1)))}{2}\right.$$

$$+ \frac{(1-p_1)(m_2p_1-m_1p_2)+m_1(p_1p_2-p_1^2)}{p_1^2(p_2-p_1)}\frac{(-\sin(2\cos^{-2}(2p_1-1)))}{2} \qquad (8)$$

$$\left. + \frac{(m_2p_1-m_1p_2)}{p_1^2(p_2-p_1)}\left[\frac{-\sin(\cos^{-1}(2p_1-1))}{2} - \frac{\sin(3\cos^{-1}(2p_1-1))}{6}\right]\right]$$

where:

$$C_l = 2\pi\left[\alpha - \frac{A_1 + A_2}{2}\right] \text{ and } \quad C_m = \pi\left[\frac{A_1 + A_2}{2}\right] \tag{9}$$

Now using the terms of C_l and C_m in terms of these coefficients for an arbitrary 10° angle of attack and for no reflex angle, the values of the coefficients became:

$$C_l = 1.8405$$

$$C_m = -.1297$$

while reference 5 showed values of:

$$C_l = 1.5500$$

$$C_m = -.1000$$

which demonstrated that the proposed model of the airfoil section was accurate enough for the purposes of this desigr. After numerous iterations of the equations to arrive at a shape that yielded the desired properties, the final result was an airfoil section with a reflex angle of 13° that started the reflex at the .8 chord point as illustrated in figure 4.

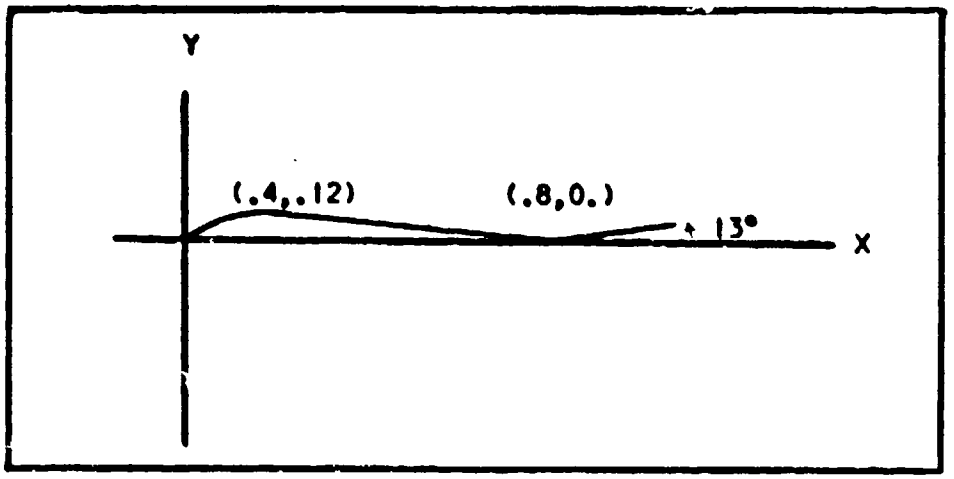

Fig. 4 Reflexed Airfoil

Although the above section characteristics could have been extended to the finite wing, it was unnecessary since wind tunnel results would yield more accurate results and would be ready for the stability analysis.

Stability Analysis

The stability analysis rested on the fact that the longitudinal stability analysis could be separated from the lateral analysis. The equations of motion used in the analysis were developed in reference 4 and the assumptions that allow the longitudinal motion to be separated from the lateral motion are discussed at length there. For the purposes of the following analysis, all of the assumptions were valid.

Longitudinal Analysis. Since static longitudinal stability could be normally achieved by ensuring that C_{M_α} is negative, the analysis of the dynamics of the vehicle also included static stability. The solution to the resulting eigenvalue problem yielded all of the required information concerning dynamic stability. The characteristic matrix resulting from the equations of motion as developed in reference 4 and after eliminating both thrust and speed derivative terms was:

$$\begin{bmatrix} \frac{C_{w_e} \sin\gamma_e}{\mu} & \frac{C_{L_e} - C_{D_\alpha}}{2\mu} & 0 & \frac{-C_{w_e} \cos\gamma_e}{2\mu} \\ \frac{2C_{w_e} \cos\gamma_e}{2\mu + C_{L_{\dot\alpha}}} & -\frac{C_{L_\alpha} + C_{D_e}}{2\mu + C_{L_{\dot\alpha}}} & \frac{2\mu - C_{L_q}}{2\mu + C_{L_{\dot\alpha}}} & \frac{-C_{w_e} \sin\gamma_e}{2\mu + C_{L_{\dot\alpha}}} \\ \frac{1}{\hat{I}_y} \frac{(-C_{M_{\dot\alpha}})(2C_{w_e} \cos\gamma_e}{2\mu + C_{L_{\dot\alpha}}} & \frac{1}{\hat{I}_y} C_{M_\alpha} - \frac{C_{M_{\dot\alpha}} (C_{L_\alpha} + C_{D_e})}{2\mu + C_{L_{\dot\alpha}}} & \frac{1}{\hat{I}_y} C_{M_q} + \frac{C_{M_{\dot\alpha}} (2 - C_{L_q})}{2\mu + C_{L_{\dot\alpha}}} & \frac{-C_{M_{\dot\alpha}} C_{w_e} \sin\gamma_e}{\hat{I}_y (2\mu + C_{L_{\dot\alpha}})} \\ 0 & 0 & 1 & 0 \end{bmatrix}$$

The assumption that the speed derivatives were negligible was warranted by the very low speed that the design criteria required.

The major difficulty in the analysis was to find reliable forms of the derivatives in terms of the planform parameters. The forms that follow are based on the assumption that the effects of the wing and body can be separated and added. This assumption remained valid throughout the range of linear aerodynamics considered in the analysis. Throughout the analysis where the derivatives depend on parameters that are defined only graphically in the references, those derivatives will be expressed as functional relationships. Where static margin was a parameter, a value of .25 was used for the derivative value shown.

C_{L_α}. This derivative represented the change in lift with changing angle of attack. The theoretical value of 2π was assumed and corrected for finite wing effects using a correction factor presented in reference 6.

$$C_{L_\alpha} = f(\gamma_a, AR) \tag{11}$$

$$C_{L_\alpha} = 4.23368$$

C_{D_α}. This derivative represented the change in drag with changes in angle of attack.

$$C_{D_\alpha} = f(C_L, C_{L_\alpha}, e, AR) \qquad \text{(Ref. 7)} \tag{12}$$

$$C_{D_\alpha} = .5091$$

C_{M_α}. This derivative represented the change in the moment coefficient with changes in angle of attack. It represented the primary factor in static stability and as such had to be negative to ensure static stability.

$$C_{M_\alpha} = -k_n C_{L_\alpha} \qquad \text{(Ref. 4)} \quad (13)$$

$$C_{M_\alpha} = -1.05842$$

$C_{L_{\dot\alpha}}$ and $C_{M_{\dot\alpha}}$. These derivatives were assumed to be negligible in a tailless design since the primary contribution to the magnitudes of the derivatives was a result of the lag in downwash reaching the tail (Ref. 4) and thus was absent in this configuration.

C_{L_q}. This derivative resulted from the change in lift due to pitching velocity.

$$C_{L_q} = f(k_n, C_{L_\alpha}) \qquad \text{(Ref. 7)} \quad (14)$$

$$C_{L_q} = 4.23368$$

C_{M_q}. This derivative resulted from the change in pitching moment due to changes in the pitching velocity. It represented the primary damping force for short period oscillations.

$$C_{M_q} = f(\Lambda, C_{L_\alpha}, k_n, AR) \qquad \text{(Ref. 8)} \quad (15)$$

$$C_{M_q} = -.993186$$

The equilibrium flight condition used in the stability analysis was:

$$C_{L_e} = .86815 \qquad C_{D_e} = .1200 \qquad \gamma_e = -7.9°$$

The characteristic matrix, eigenvalues, and eigenvectors were calculated by a digital computer program written for this purpose and Argand diagrams of the eigenvectors are presented in Appendix A. A root locus of the eigenvalues for a range of static margin from .05 to .30 for the short period is presented in figure 5a and for the phugoid in figure 5b. It can be seen that the longitudinal modes were both stable and thus represented satisfactory solutions to longitudinal stability.

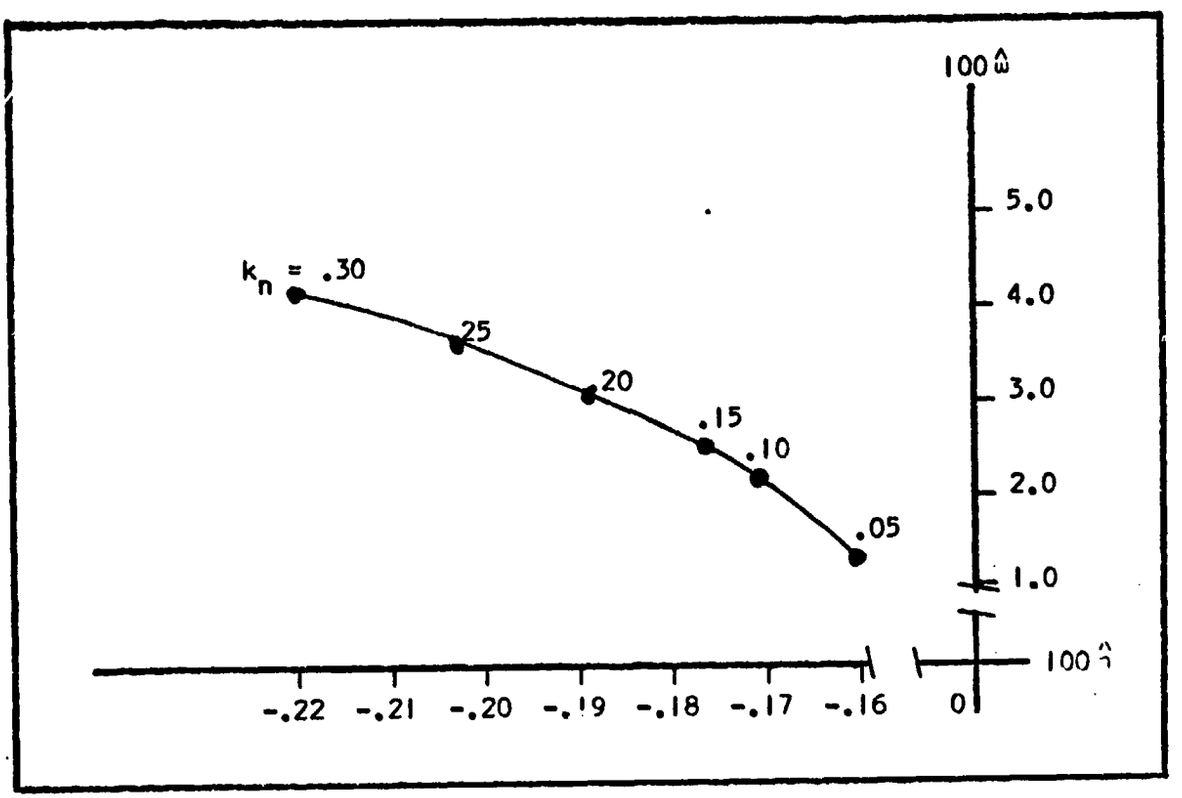

Fig. 5a Root Locus Wing-Body - Short Period

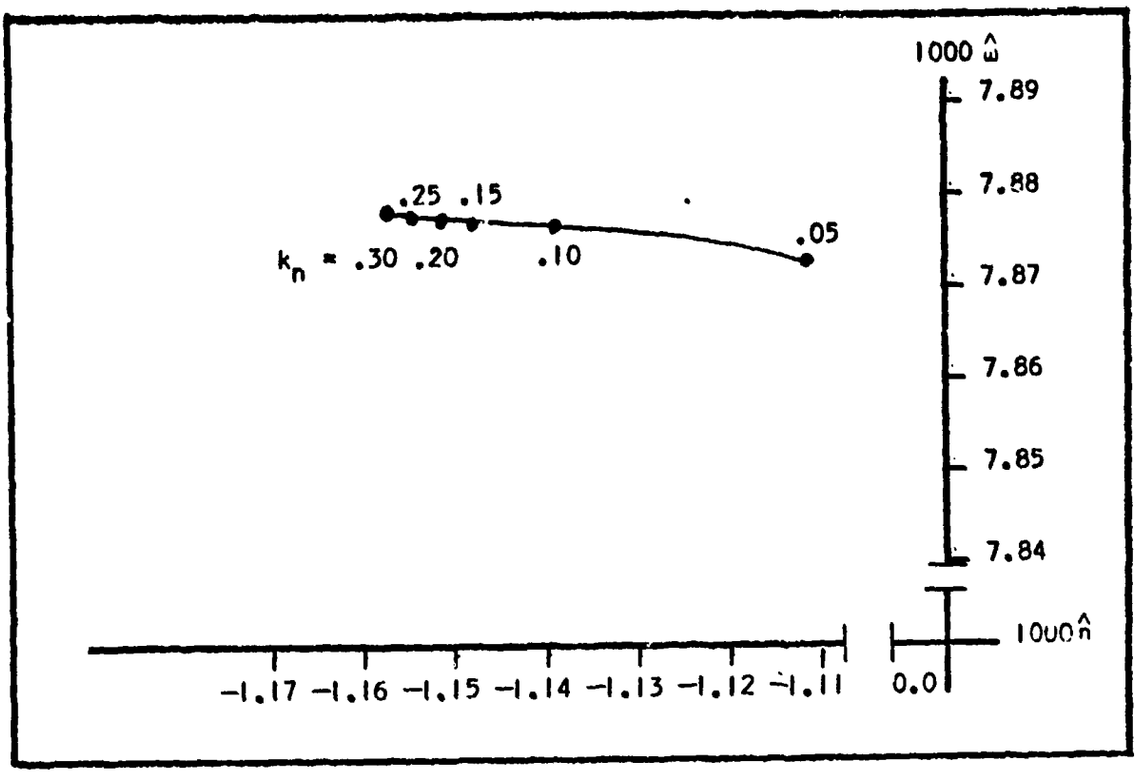

Fig. 5b Root Locus for Wing-Body - Phugoid

Lateral Analysis. The lateral equations of motion from the same reference as for the longitudinal equations were utilized in the analysis and after making the same assumptions as in the longitudinal case the characteristic matrix became:

$$\begin{bmatrix} \frac{C_{Y_\beta}}{2\mu} & \frac{C_{Y_p}}{2\mu} & \frac{C_{Y_r} - 2\frac{\mu}{AR}}{2\mu} & \frac{C_{w_e}\cos\gamma_e}{2\mu} \\ \frac{C_{l_\beta}}{\hat{i}_x^{\prime}} & \frac{C_{l_p}}{\hat{i}_x^{\prime}} & \frac{C_{l_r}}{\hat{i}_x^{\prime}} & 0 \\ \frac{C_{n_\beta}}{\hat{i}_z^{\prime}} & \frac{C_{n_p}}{\hat{i}_z^{\prime}} & \frac{C_{n_r}}{\hat{i}_z^{\prime}} & 0 \\ 0 & \frac{1}{AR} & \frac{1}{AR}\tan\gamma_e & 0 \end{bmatrix}$$

Utilizing the same equilibrium conditions as in the longitudinal case, the lateral derivatives were calculated in the following manner.

C_{Y_β}. This derivative represented the change in side force due to sideslip. The major contributions were from body effects with small effects from the wing. The best representation for this derivative was created by summing dihedral and body effects from reference 8 with the wing effects presented in reference 7.

$$C_{Y_\beta} = f(\Gamma, S_0, S, C_{L_e}, \Lambda, AR) \tag{17}$$

$$C_{Y_\beta} = .324182$$

Although typical values of this derivative are negative, these values arise from tail effects which overcome the destabilizing effects of the body and are not present in this configuration.

C_{l_β}. This derivative was of paramount concern in this design since it was the major determinent of directional stability; one of the critical design points. The major influences in this derivative were from wing sweep, dihedral, and aspect ratio. The form used for this derivative was a summation of body and dihedral effects from reference 8 with the wing effects from reference 7.

$$C_{l_\beta} = f(\Lambda, \Gamma, AR, b, d, C_{L_e}, z_w) \tag{18}$$

$$C_{l_\beta} = -.12885$$

C_{n_β}. This derivative provided the yaw stiffness to the vehicle and a such had to be positive or the vehicle would have been statically unstable in yaw. Normally the effects of the body would have outweighed the effects of the wing because of a large body area ahead of the center of gravity; however, in this case the wing effects outweighed the body effects and caused the value to favor static stability. Contributions from the body were evaluated using the methods of reference 8 while wing effects were calculated from methods of reference 7.

$$C_{n_\beta} = f(S, l_B, C_L, \Lambda, AR, k_n) \qquad (19)$$

$$C_{n_\beta} = 8.8073 \times 10^{-3}$$

C_{y_p}. This derivative represented the change in the sideforce with the change in wing-tip helix angle (Ref. 3). The wing contributed the major effects to this derivative and since experimental evidence indicated that the body effects were negligible (Ref. 3), only wing effects were calculated.

$$C_{y_p} = f(C_L, AR, \Lambda) \qquad \text{(Ref. 7)} \quad (20)$$

$$C_{y_p} = .158657$$

C_{n_p}. This derivative represented the yawing moment caused by roll and caused the close coupling of roll and yaw (Ref. 3). In the case of this configuration, these effects were more closely coupled than normal, which made any lateral instabilities difficult to analyze and correct.

In this case experimental evidence allowed the effects of the body to be neglected (Ref. 3).

$$C_{n_p} = f(AR, \Lambda, k_n, C_L) \qquad \text{(Ref. 7)} \qquad (21)$$
$$C_{n_p} = -.14163$$

It should be noted that C_{n_p} varies with C_L as shown in reference 3 and therefore could have been of either sign. The negative sign in the present case was destabilizing and no method of changing its sign could be found without flying at a C_L that was unacceptable from a performanc consideration.

C_{y_r}. This derivative represented the change in sideforce with variations in yawing velocity.

$$C_{y_r} = f(C_L, \Lambda, AR, k_n) \qquad \text{(Ref. 7)} \qquad (22)$$
$$C_{y_r} = -.03324$$

C_{n_r}. This derivative represented the effects of asymmetrical lift and drag distribution over the wing during yaw (Ref. 3). In the present case the effects of the body were possibly significant (Ref. 3), but no known method of calculating these effects was known (Ref. 3). The value of this derivative was similar to values in reference 9 so the value was assumed to be approximately correct.

$$C_{n_r} = f(C_L, AR, k_n, C_{D_e}, \Lambda) \text{ (Ref. 7)} \qquad (23)$$
$$C_{n_r} = -.030108$$

C_{l_p}. This derivative represented the change in rolling moment coefficient with the change in wing-tip helix angle and in this case experimental evidence indicated that body effects were negligible (Ref. 3).

(Ref. 7) (24)

$$C_{l_p} = -.405159$$

C_{l_r}. This derivative represented the rolling moment due to yaw rate. Fuselage effects could also be neglected in this case (Ref. 3)

(Ref. 7) (25)

$$C_{l_r} = .23995$$

The equilibrium conditions for the lateral analysis were the same as those used in the longitudinal analysis. A root locus for the dutch roll for a static margin range from .05 to .30 is shown in figure 5c. Argand diagrams for the static margin range are shown in Appendix B. As shown in the root locus below, the vehicle was found unstable in dutch roll. No method was found to stabilize the analytical model of the vehicle from changes in the vehicle parameters, such as wing configuration, mass, moments of inertia, or body shape.

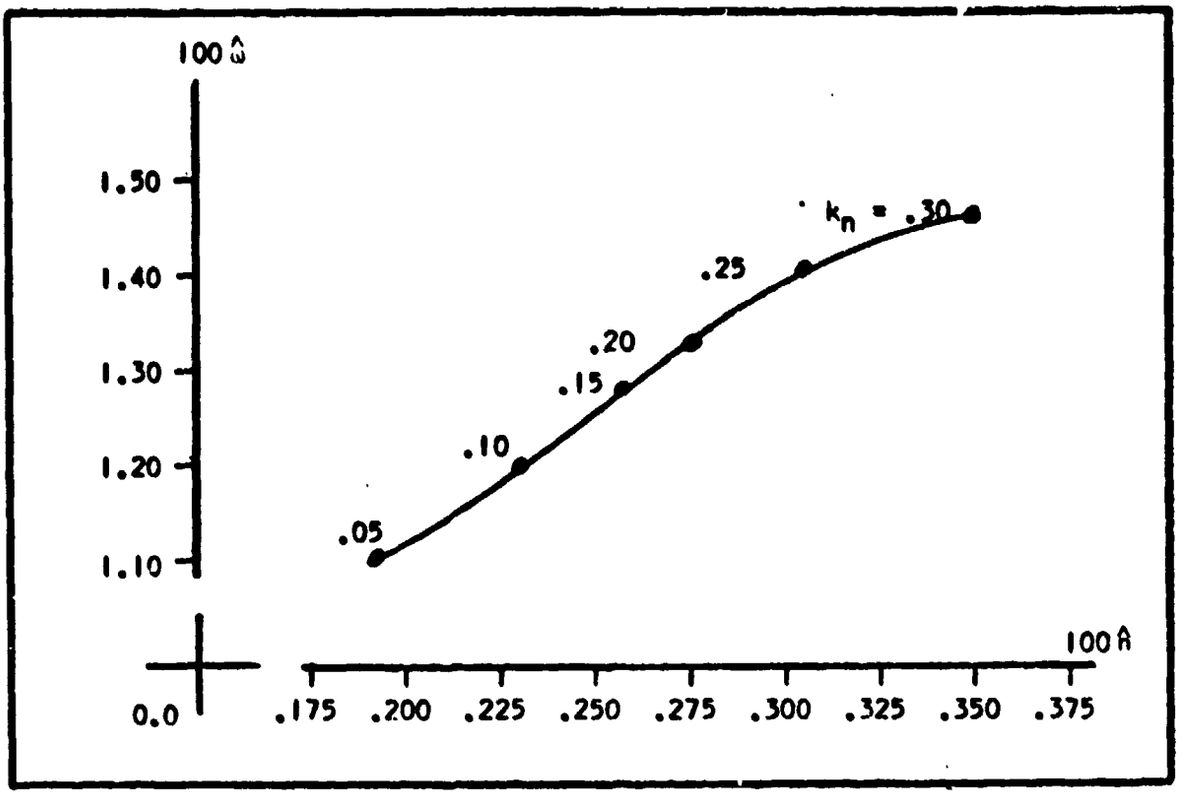

Fig. 5c Root Locus for Wing-Body - Dutch Roll

Wind Tunnel Tests

Wind tunnel tests were performed in an attempt to validate the analytical model, find possible corrective measures for the apparent lateral instability, and to provide information in areas not covered by the analytical model. The tests were performed in the AFFDL one-meter low speed wind tunnel; a closed loop, constant speed tunnel. All data runs were conducted at the tunnel airflow maximum speed of 75fps., which closely simulated the analytical model's 84 fps. Runs were made to measure both lift and drag, with moment data unavailable due to equipment malfunction. Curves showing the data are presented in figure 6.

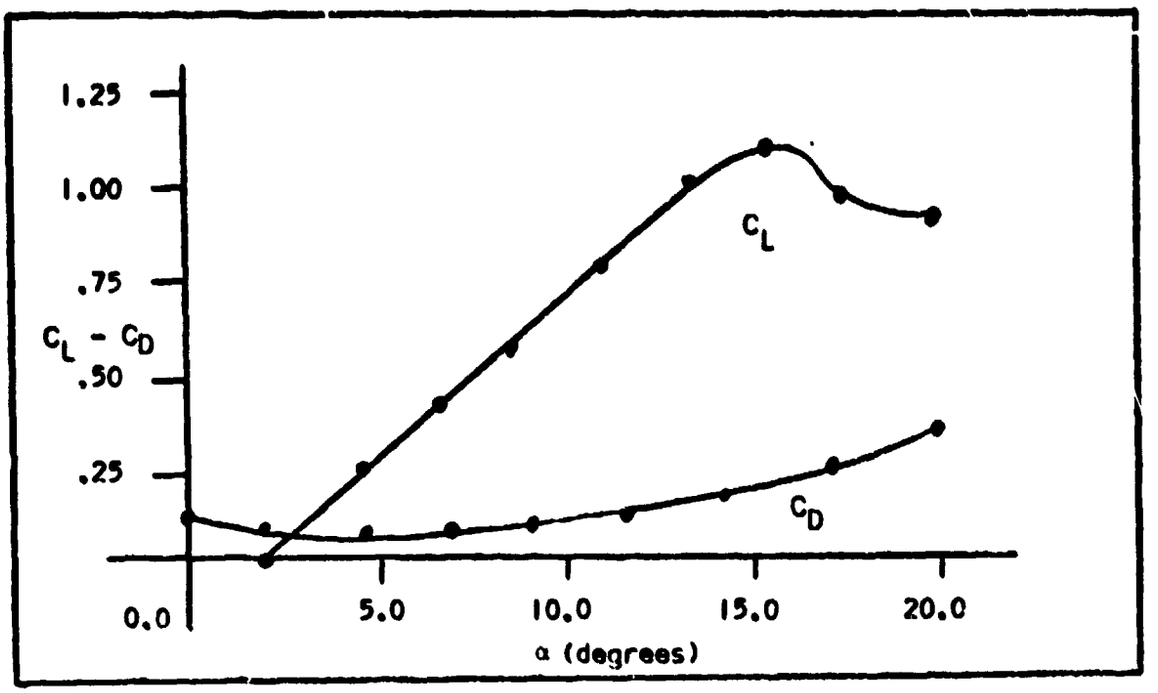

Fig. 6 Wing-Body Lift and Drag Curves

As seen in figure 6, both C_L and C_D are within 20% of that predicted by the theoretical model. Three further studies were performed to investigate model performance and to partially validate the theoretical model.

The first of these runs was performed after tufting the model to investigate the airflow around the model. This test was performed at angles of attack of 10°, 15°, and 20° to validate the analytical model in flight conditions around the equilibrium position. Very smooth airflow was observed over the surface of the entire vehicle, in particular around the wing body juncture. This area of smooth flow helped to validate the assumption that body and wing effects could be calculated separately and added together.

The second run was performed in a one-degree of freedom mount (Fig.7) to test longitudinal stability.

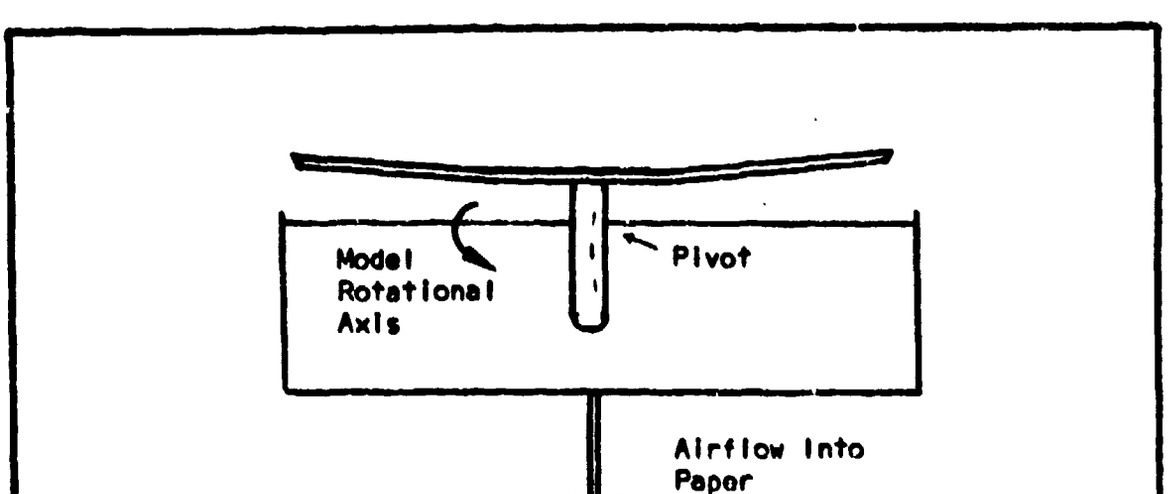

Fig. 7 One Degree of Freedom Longitudinal Mount

This run enabled both the trim angle of attack to be found for this dynamic pressure and the reflex angle chosen for the camber line to be tested. As the airflow was started, the model trimmed at an angle of attack of 12° and was very stable in pitch. Motions induced by interruptions in the airflow were damped out rapidly as predicted by the short period eigenvalue analysis. In this case both the reflex angle predicted and the short period response were validated by the experimental evidence.

The third test was conducted in a similar manner to that of the short period test with the exception that the model was mounted in a fitting that allowed freedom around the z-axis (Fig. 8). Although friction in the mounting bearing could have affected the damping, it could not have provided a restoring force so this run demonstrated the directional stability of the vehicle, since the model trimmed straight ahead and any perturbations were damped out rapidly. None of the closely coupled modes of the analytical model were able to be completely validated due to a lack of sufficient degrees of freedom in the tunnel mounts.

The major conclusions provided by the wind tunnel tests were the

lift and drag data, and partial validation of the analytical model. In particular, the longitudinal short period mode was validated as was the airfoil design. No tests could be devised with the available equipment to test the unstable lateral mode, so no conclusions could be made concerning total vehicle stability or methods to correct the lateral instability predicted by the analytical model.

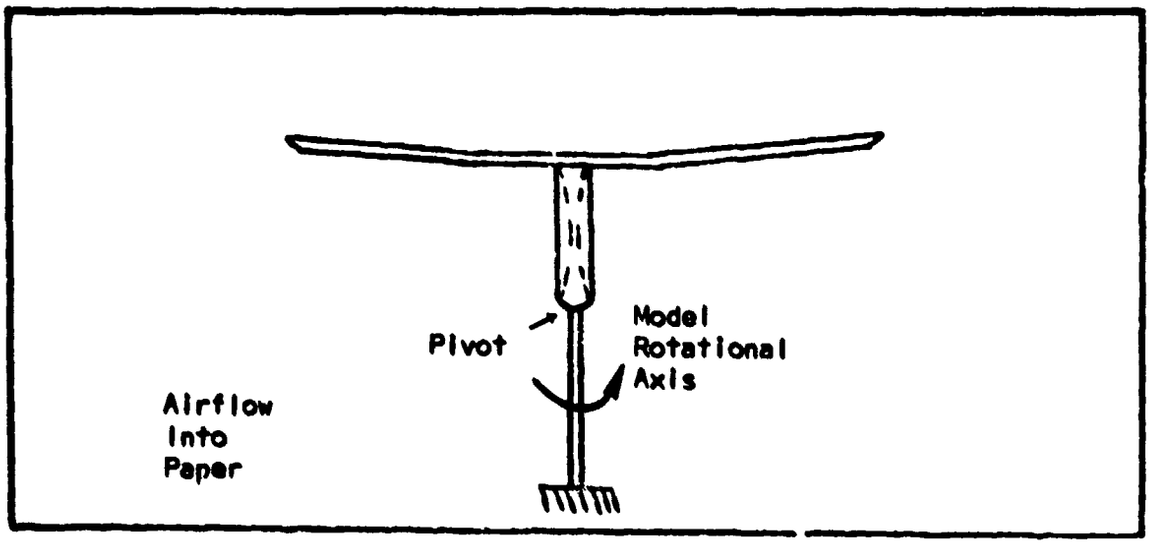

Fig. 8 One Degree of Freedom Lateral Mount

Moment of Inertia Calculation

The following method of moment of inertia calculation was discussed extensively in reference 10. For inertia measurement about the y-axis, a pivot was inserted into the model fuselage at right angles to the x-axis and vertically above the longitudinal center of gravity position. The model was then suspended from this pivot at a distance l from the center of gravity so the model oscillated about an axis parallel to the y-axis. The moment of inertia about the y-axis was then:

$$I_{yy} = \frac{T^2 wl}{4\pi^2} - \frac{wl^2}{g} \qquad (26)$$

I_{yy} was also a principal moment due to the x-z plane of symmetry. The period was determined to an accuracy of .1% by timing 50 oscillations with a stopwatch.

To determine the principal axes orientation, the model was set at a series of small pitch angles to the horizontal and the rolling moment of inertia was determined at each attitude by the above method. The minimum rolling moment of inertia obtained in this manner was the principal rolling moment of inertia and the angle with the horizontal gave the orientation of the principal axes. The results of this calculation indicated that the y-z plane was also mass symmetric, therefore all three axes were principal axes.

The yawing moment of inertia was determined by swinging the model as a torsional pendulum, using a bi-filar suspension. The two wires were attached to the x-axis an equal distance fore and aft of the center of gravity. Then the yawing moment was:

$$I_{zz} = \frac{wT^2 d}{4\pi^2 l} \tag{27}$$

These inertias were corrected for center of gravity location for the various static margins and non-dimensionalized using the non-dimensionalization from reference 4 so that they would be compatible with those equations. For a static margin of .25 the input inertias were:

$$\hat{I}_{xx}' = 33.209$$
$$\hat{I}_{yy}' = 770.120$$
$$\hat{I}_{zz}' = 35.112$$

Flight Test

This portion of the analysis was performed by hand launch from a helicopter moving at a forward velocity of 60 knots and flying at an altitude of 750 ft. These tests showed that the vehicle was very unstable, in what appeared to be the dutch roll mode, although this observation was very subjective. Since these tests confirmed that the vehicle was unstable as predicted by the analytical model, some type of vehicle modification was required to achieve stability.

New Configurations

Three types of modifications were tried in an attempt to stabilize the vehicle. The first of these was the addition of a vertical stabilizer to the rear of the model. This configuration was tunnel tested and it appeared to damp out the perturbations in sideforce more rapidly than the basic vehicle. When this vehicle was flight tested very little improvement was noted, so without a longer tail moment arm this modification was insufficient. The next two attempts were similar in intent. In an attempt to prevent the vehicle from entering the oscillations, two types of drag devices were tried. The first was a ribbon parachute 2" wide and 12" long. The second device was a conical rigid parachute 2" in diameter attached by a 12" thread to the rear of the vehicle on an axis through the center of gravity. In both cases the additional drag was so large that the weight component was insufficient to provide flying airspeed.

Conclusions

After the last tests of the vehicle, it was decided that this

configuration would not be further investigated. It was unlikely that a stable form of this configuration could be developed, and even if marginal stability were achieved, it would not be as satisfactory a configuration as the conventional vehicle.

IV. THE WING-BODY-TAIL DESIGN

As major stability problems began to appear in the wing-body analysis, more emphasis was placed on the wing-body-tail design study. The first step in the design process was to define in exact terms the planform parameters for the first iteration of the wing-body-tail analysis.

Tail Design

The best location from stability considerations of the tail-boom body juncture was high on the body (Ref. 11). This study of a similar configuration found that the vehicle had greater lateral stability with the tail-boom located high on the body, primarily due to the elimination of body-tail interference at some high angles of attack. Therefore, the tail-boom was mounted just below the wing trailing edge as shown in figure 2. It was seen in the wind tunnel tests of this configuration that this location did eliminate body-tail interference as desired.

The specific details of the tail design were arrived at from an evaluation of the packaging problem. The first tail-boom folding mechanism considered was a pivot at the body-boom juncture with the boom being constructed from a material with sufficient flexibility to allow it to be wrapped around the circumference of the body. The only practical vertical tail planform useable with this tail-boom design was a twin vertical tail with the vertical stabilizers located at the extreme ends of the horizontal stabilizer. To provide the maximum available horizontal stabilizer span, the span was chosen so that the vertical stabilizers would fit outside of the wings when folded.

Tail-boom length was chosen as a compromise between boom flexibility and tail sensitivity. Since the tail-boom was to be flexible, the shorter

the tail-boom within the limits of stability, the less sensitive the vehicle would be to tail deformation. For this reason, a tail-boom length of 9" was chosen as the starting point in the design process. Both horizontal stabilizer chord and vertical tail area were chosen to provide a tail volume of slightly over .5 since the tail volume of the configuration in reference 11 was approximately this value.

Stability Analysis

The same assumptions made in the wing-body analysis were necessary in developing this analytic model, except where less stringent assumptions were allowable as noted in the analysis. One further assumption was made concerning flow at the tail. It was assumed that the tail was located in an area of undisturbed flow except for the downwash effects on the tail angle of attack. The evidence of reference 11 indicated that this was a valid assumption. The same equations of motion and the same resulting characteristic matrix as used in the wing-body analysis were used in this analysis and therefore will not be repeated.

Longitudinal Analysis. The equilibrium conditions used in this analysis were similar to those used in the wing-body analysis and are not repeated. Where the stability derivatives are a function of static margin, a static margin of .25 was chosen for demonstration purposes. All of the following derivatives and those in the lateral analysis were calculated using the methods of reference 8.

C_{L_α}.

$$C_{L_\alpha} = f(AR, S_H, C_{l_{\alpha_w}}, C_{l_{\alpha_H}}) \tag{28}$$

$$C_{L_\alpha}\Big|_{\text{Theory}} = 4.524$$

$$C_{L_\alpha}\Big|_{\text{Wind tunnel}} = 4.756$$

The value of 2π was assumed as the horizontal stabilizer C_{l_α} because of the endplate effects of the vertical stabilizer. As seen from the wind tunnel test data the resulting value was quite good using this assumption.

C_{D_α}.

$$C_{D_\alpha} = f(C_L, C_L, AR) \tag{29}$$

$$C_{D_\alpha}\Big|_{\text{Theory}} = .64848$$

$$C_{D_\alpha}\Big|_{\text{Wind tunnel}} = .1203$$

The predicted value was not very good in this case. Since the forms of the derivatives used in this analysis were empirical curve fits to conventional data sets, it is possible that the lack of a conventional fuselage resulted in an artificially high value being predicted.

C_{M_α}.

$$C_{M_\alpha} = f(C_{L_\alpha}, k_n) \tag{30}$$

$$C_{M_\alpha} = -1.1890$$

C_{l_q}.

$$C_{l_q} = f(C_{l_{\alpha_w}}, C_{l_{\alpha_H}}, k_n, \bar{V}_H) \tag{31}$$

$$C_{l_q} = 9.8775$$

C_{M_q}.

$$C_{M_q} = f(C_{l_{\alpha_w}}, C_{l_{\alpha_H}}, k_n, \bar{V}_H, AR) \tag{32}$$

$$C_{M_q} = -19.157$$

$C_{L_{\dot{\alpha}}}$. The value for this derivative could only be calculated for the tail effects and was thus multiplied by a factor of 1.1 (Ref. 4).

$$C_{L_{\dot{\alpha}}} = f(C_{l_{\alpha_H}}, \bar{V}_H, \frac{d\epsilon}{d\alpha}) \tag{33}$$

$$C_{L_{\dot{\alpha}}} = 2.5222$$

$C_{M_{\dot{\alpha}}}$.

$$C_{M_{\dot{\alpha}}} = f(C_{l_{\alpha_H}}, \bar{V}_H, \frac{d\epsilon}{d\alpha}) \tag{34}$$

$$C_{M_{\dot{\alpha}}} = -7.115$$

The value of the pitching moment was calculated by the same methods used for the wing body.

$$\hat{I}_y = 2499.4$$

The resulting eigenvalues and eigenvectors for a static margin of .25 :

Short Period: $-6.7864\times10^{-3} \pm 2.1198\times10^{-2}\,i$ $\quad \zeta = .3049$

$\hat{V}$:	$2.6008\times10^{-3} \mp 1.5650\times10^{-3}\,i$
α:	$4.5040\times10^{-1} \mp 5.5652\times10^{-1}\,i$
$\hat{q}$:	$1.0215\times10^{-2} \pm 1.1705\times10^{-2}\,i$
θ:	$3.6909\times10^{-1} \mp 5.9744\times10^{-1}\,i$

Phugoid: $-5.5226\times10^{-5} \pm 7.7737\times10^{-4}\,i$ $\quad \zeta = .0709$

$\hat{V}$:	$4.5196\times10^{-1} \mp 3.7087\times10^{-1}\,i$
α:	$-8.6222\times10^{-3} \pm 5.3903\times10^{-3}\,i$
$\hat{q}$:	$5.0104\times10^{-4} \mp 3.8555\times10^{-4}\,i$
θ:	$-5.3904\times10^{-1} \mp 6.0623\times10^{-1}\,i$

The root locus for a static margin range of .05 to .30 for the short period is shown in figure 9a and for the phugoid in figure 9b. Argand diagrams for the static margin range are presented in Appendix C. As shown, the vehicle was stable in both longitudinal modes; however, the phugoid was weakly damped so further studies were made of the sensitivity of the analytical model to changes in the derivative values.

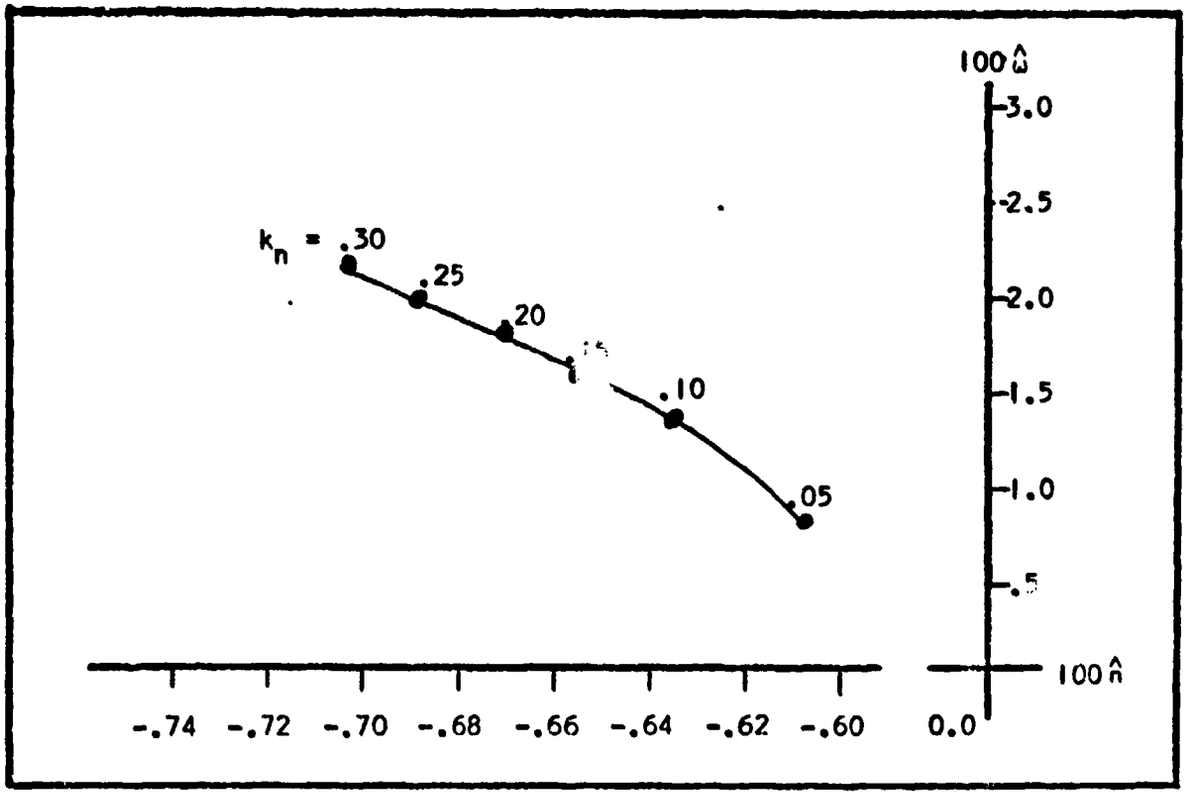

Fig. 9a Root Locus for Wing-Body-Tail - Short Period

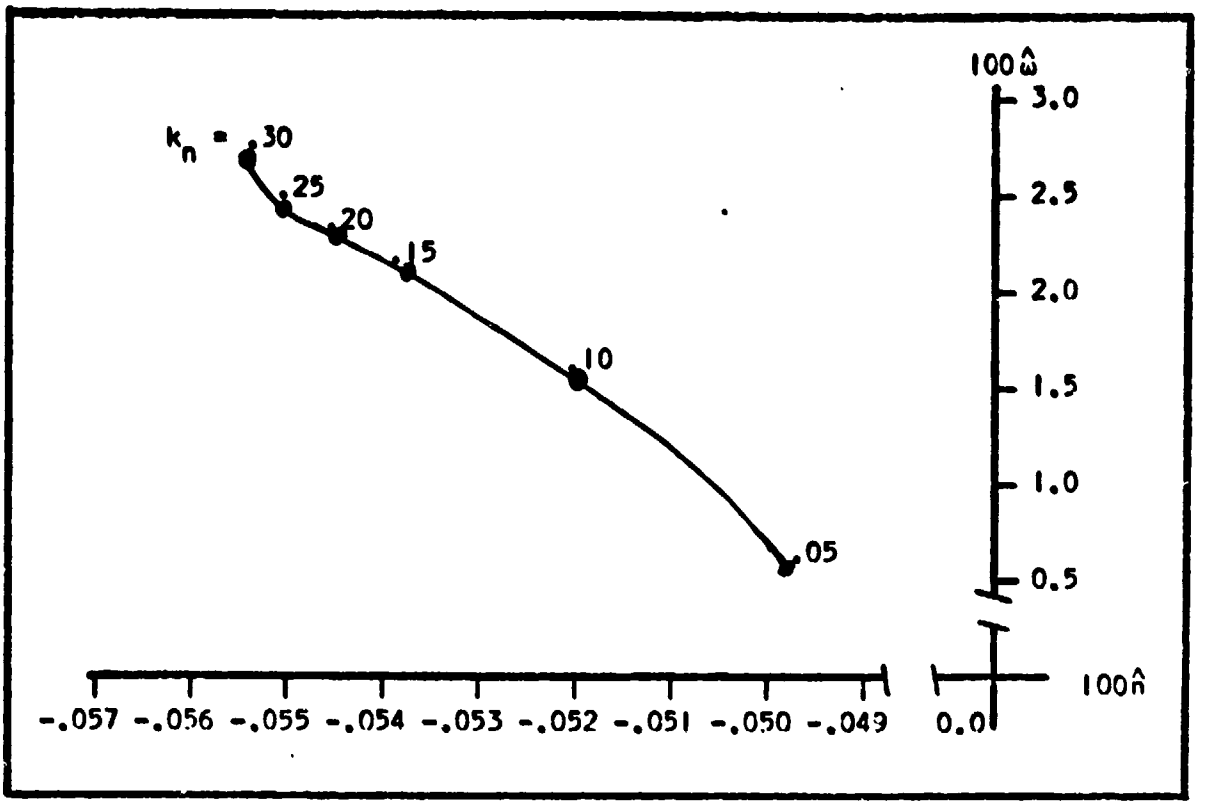

Fig. 9b Root Locus for Wing-Body-Tail - Phugoid

Longitudinal Sensitivity Analysis. Two results were obtained from this analysis: 1) the sensitivity of the model to errors in the derivatives was evaluated, and 2) possible methods to increase phugoid damping were found. The changes in each derivative and the resulting eigenvalues are shown in Appendix D.

It was seen from this analysis that the model was relatively insensitive to derivative errors since only small variations in response occurred and the model remained stable for all variations. The only derivative that made noticeable changes in the phugoid was C_{m_q} (other than C_L which could not be easily changed) and even this derivative made only minor changes in the phugoid. However, as a result of this possible improvement in response, two different attempts were made to increase

phugoid damping. The first change was an increase in the horizontal stabilizer chord to 3". The second change was to increase tail volume to .8, which although similar to changing the chord, could be arrived at by other means including lengthening the tail-boom, or increasing the horizontal tail span. Neither of these two changes made a noticeable change in the phugoid response.

One completely different analysis was made by assuming that the phugoid response was simply an energy transfer between the potential and kinetic energies (Ref. 4). Using this representation of the phugoid, it was possible to see one further change that would definitely increase the phugoid damping. The change was to increase the drag of the vehicle, which although undesirable from a performance standpoint, could easily be adopted if necessary. The results of increasing the drag coefficient to .12 and reducing the lift coefficient to .7 to increase the flight path angle so that the weight component would balance the increase in drag were:

Short Period:	-6.7859×10^{-3}	$2.1195\times10^{-2}i$	$\zeta = .3049$
Δ:	2.5799×10^{-3}	$1.0985\times10^{-3}i$	
α:	4.4371×10^{-1}	$5.6175\times10^{-1}i$	
$\hat{q}$:	1.0353×10^{-2}	$1.1583\times10^{-2}i$	
θ:	3.5384×10^{-1}	$6.0175\times10^{-1}i$	
Phugoid:	-1.1523×10^{-4}	$6.2474\times10^{-4}i$	$\zeta = .18064$
Δ:	5.7758×10^{-1}	$8.8540\times10^{-2}i$	
α:	-8.2241×10^{-3}	$2.6877\times10^{-4}i$	
$\hat{q}$:	5.1707×10^{-4}	$2.4096\times10^{-5}i$	
θ:	-1.8358×10^{-1}	$7.9044\times10^{-1}i$	

As shown, this change resulted in a major change in the phugoid response; however, the glide ratio was reduced by 50% to 5.8. This glide ratio was acceptable to meet the performance requirements if that large of a trade-

off in performance was necessary to obtain the desired response. As a result of this study, it was decided that the original phugoid response would be retained unless flight tests showed that it was unacceptable.

Aeroelastic Analysis. The influence of tail-boom flexibility was considered to have a major impact on vehicle stability because of the proposed tail packaging concept. The following analysis was conducted under the assumption that the tail flexibility could be represented by assuming that a torsional spring located at the pivot provided all of the flexibility to the boom, while the rest of the boom was assumed to be rigid. This assumption was valid because the only significant change occurring because of tail flexibility was a change in the angle of attack of the tail relative to the vehicle, and no significant effects were caused by the boom itself. The following analysis follows that of reference 4 closely. Assume that $\nabla\alpha_t = -kL_t$ where k is the flexibility of the torsional spring located at the pivot. The figure below illustrates the assumed model.

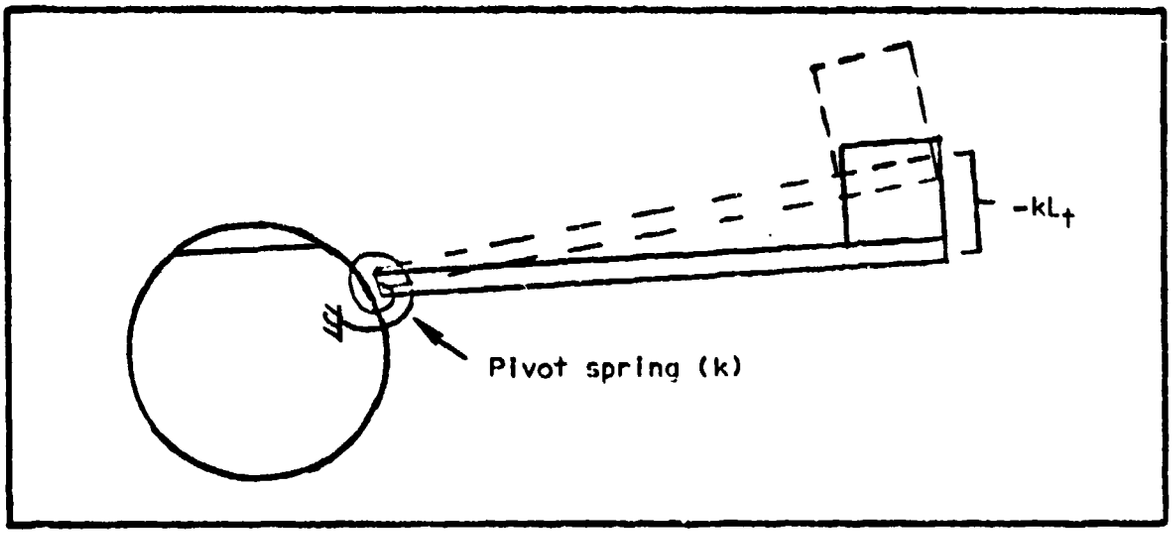

Fig. 10 Aeroelastic Model

let: $$a_t = C_{L_{a_t}} (a_{WB} - \epsilon - kL_t) \quad (35)$$

then: $$C_{L_t} = \frac{C_{L_{a_t\ rigid}}}{1 + kC_{L_{a_t\ rigid}} (.5\rho V^2 S)} (a_{WB} - \epsilon) \quad (36)$$

and the tail effectiveness has been reduced by a factor of:

$$\frac{1}{1 + kC_{L_{a_t\ rigid}} (.5\rho V^2 S)} \quad (37)$$

After this factor was substituted into the appropriate places in the stability analysis, the following reductions in static margin were found for the flexibility values shown at the basic static margin of .25:

$$k_{basic} = .05906 \text{ (flight test model flexibility)}$$

$$\Delta k_n = .06$$

$$k = .08818 \ (1.5\ k_{basic})$$

$$\Delta k_n = .08$$

$$k = .03937 \ (k_{basic} / 1.5)$$

$$\Delta k_n = .04$$

The changes in the static margin were significant for the case where either payload requirements required a low static margin to meet the packaging requirement, or the choice of a material for the tail-boom had more flexibility than evaluated in the above analysis thus resulting in a greater decrease in static margin than predicted. The solution to this problem will be further discussed in the iteration phase.

Lateral Stability Analysis. The same equilibrium conditions used in the longitudinal analysis were used in the following analysis.

C_{Y_β}.

$$C_{Y_\beta} = f(S_\Omega, S, S_v, C_{Y_{\beta_v}}) \tag{38}$$

where: $C_{Y_{\beta_v}} = f(AR_{v_t}, \Lambda_{v_t}, C_{L_{\alpha_{v_t}}})$

$C_{Y_\beta} = -.80262$

C_{l_β}

$$C_{l_\beta} = f(C_{L_{WB}}, AR, z_v, l_v, C_{Y_{\beta_v}}, \Gamma, \Lambda, \alpha) \tag{39}$$

$C_{l_\beta} = -.12442$

C_{n_β}

$$C_{n_\beta} = f(S_B, S, l, l_v, z_v, C_{Y_{\beta_v}}, \alpha) \tag{40}$$

$C_{n_\beta} = .05487$

C_{Y_p}.

$$C_{Y_p} = f(z_v, l_v, C_{Y_{\beta_v}}, \alpha) \tag{41}$$

$C_{Y_p} = .02496$

C_{l_p}.

$$C_{l_p} = f(b_H, z_v, S_H, S, C_{Y_{\alpha_v}}) \tag{42}$$

$C_{l_p} = -.42050$

C_{n_p}.

$$C_{n_p} = f(C_{l_{p_w}}, C_L, l_v, z_v, C_{y_{\beta_v}}, \alpha) \quad (43)$$

$$C_{n_p} = -.12461$$

C_{y_r}.

$$C_{y_r} = f(l_v, z_v, C_{y_{\beta_v}}, \alpha) \quad (44)$$

$$C_{y_r} = .44660$$

C_{l_r}.

$$C_{l_r} = f(C_L, l_v, z_v, C_{y_{\beta_v}}, \alpha) \quad (45)$$

$$C_{l_r} = .22013$$

C_{n_r}.

$$C_{n_r} = f(C_L, C_{D_o}, l_v, z_v, C_{y_{\beta_v}}, \alpha) \quad (46)$$

$$C_{n_r} = -.26846$$

The resulting eigenvalues for this analysis were:

Dutch Roll	Rolling Convergence	Spiral
$4.0907\times10^{-4} \pm 8.1172\times10^{-3}$ i	-4.4639×10^{-3}	-2.7798×10^{-4}

The resulting root locus for the dutch roll mode is shown in figure 11.

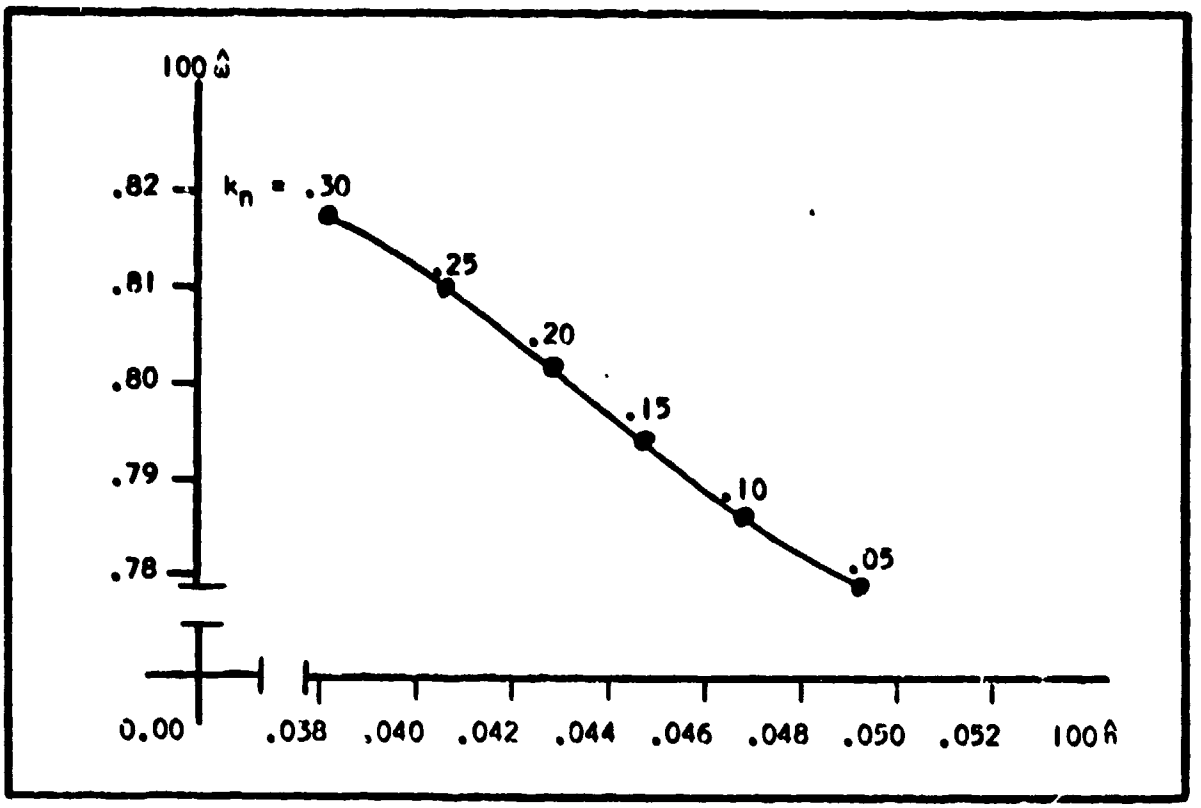

Fig. 11 Root Locus for Wing-Body-Tail for Dutch Roll I

Argand diagrams for the static margin range are presented in Appendix E. As shown in the response, the dutch roll was unstable. To find possible solutions to the instability other than an excessively large static margin which would have required the addition of wing sweep and to evaluate model sensitivity to derivative errors, a sensitivity analysis of the effects of the variation of the individual derivatives on the lateral response was made.

Lateral Sensitivity Analysis. The amount of derivative variation and the resulting eigenvalues is shown in Appendix F. The results of this analysis showed that the error sensitivity was minimal except in the case of C_{l_β} and that this derivative was the only derivative within the variation

studied that caused vehicle stabilization.

The result obtained from the sensitivity analysis was confirmed by the approximate solution to the dutch roll (Ref. 4)

$$\hat{n}_{DR_{approx}} = 1/2 \left[\frac{C_{y_\beta}}{2\mu} + \frac{C_{n_r}}{\hat{i}''_z} + \frac{\hat{i}''_z}{\hat{i}''_x} \frac{C_{l_\beta}}{C_{n_\beta}} \left(\frac{C_{n_p}}{\hat{i}''_z} - \frac{C_{w_e}}{2\mu} \right) \right] \qquad (47)$$

$$\hat{n}_{DR_{approx}} = 4.1736 \times 10^{-4}$$

$$\hat{n}_{DR_{analyt}} = 4.0907 \times 10^{-4}$$

This approximation also indicated that increases in C_{y_β}, C_{n_r}, and C_{n_β} would result in a stable dutch roll mode. After investigating the functional dependence of each of the concerned derivatives, it was determined that a change in vertical stabilizer chord would cause the desired variation in all of the necessary derivatives. Therefore, an increase in chord to 3" was evaluated. The resulting eigenvalues and eigenvectors were:

	Dutch Roll		Rolling Convergence	Spiral
	-2.6063×10^{-4}	8.9179×10^{-3} i	-3.8532×10^{-3}	-2.6755×10^{-4}
β:	3.5547×10^{-1}	4.5351×10^{-1} i	-4.6413×10^{-2}	1.1013×10^{-2}
$\hat{p}$:	1.9794×10^{-2}	3.0243×10^{-2} i	-2.0062×10^{-2}	-1.1998×10^{-3}
$\hat{r}$:	-1.9655×10^{-2}	1.8271×10^{-2} i	2.0508×10^{-3}	2.9588×10^{-4}
θ:	6.5921×10^{-1}	4.7111×10^{-1} i	9.9872×10^{-1}	9.9993×10^{-1}

The resulting root locus for the entire static margin range is shown in figure 12.

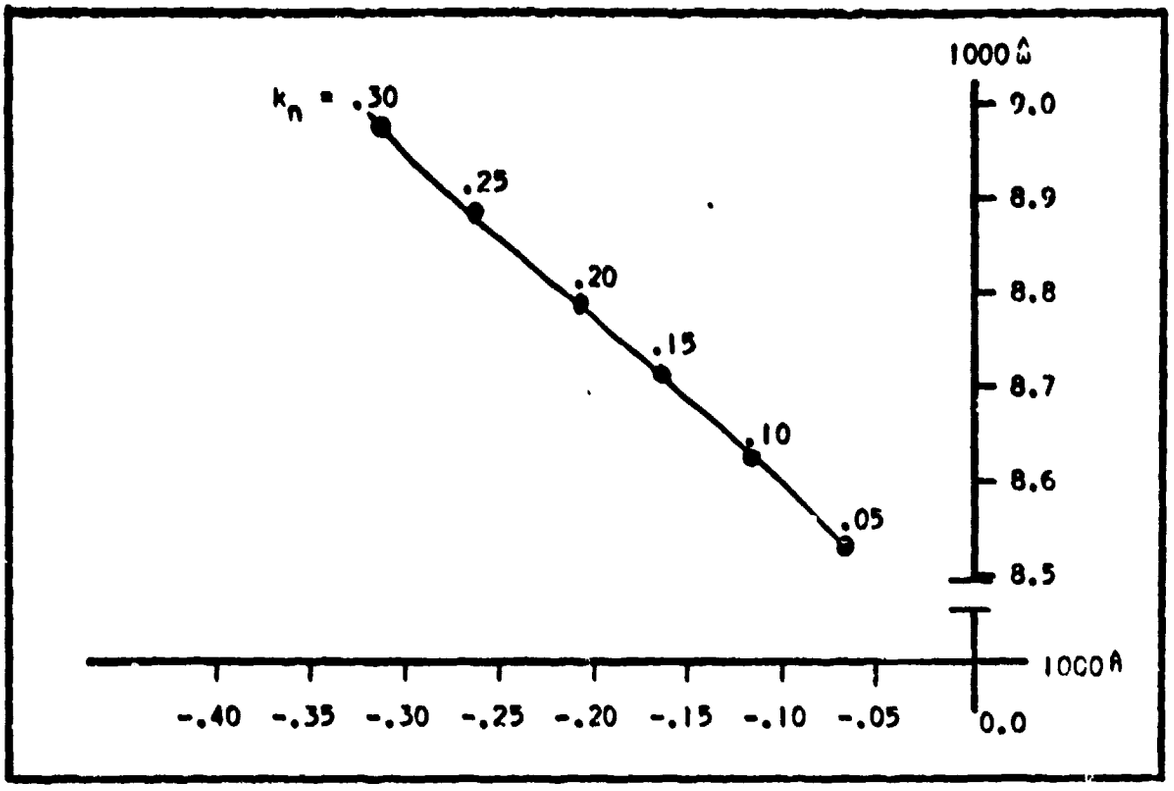

Fig. 12 Root Locus for Wing-Body-Tail - Dutch Roll 2

The resulting response was stable as desired and, although the dutch roll was of long period, it was satisfactory to meet the design requirements. The response for the static margin range is presented in Appendix G.

The effects of altitude which were important in this design were discussed at length in reference 4 and since they mainly enter through the non-dimensionalization of the terms, they were not studied explicitly. As discussed in reference 4, the effects of altitude variation were mainly to reduce damping as altitude was increased and to increase the period of both the phugoid and the dutch roll modes. Although these effects were undesirable, the only correction for these effects was to make the finalized vehicle as heavily damped as possible in these two modes without sacrificing stability in the remaining modes.

Wind Tunnel Tests

The same set of wind tunnel tests were run for the wing-body-tail configuration as were run for the wing-body configuration. Both lift and drag were measured, and the other tests to evaluate the analytical model and the assumptions necessary in its development were run. The lift and drag curves that resulted are shown in figure 13.

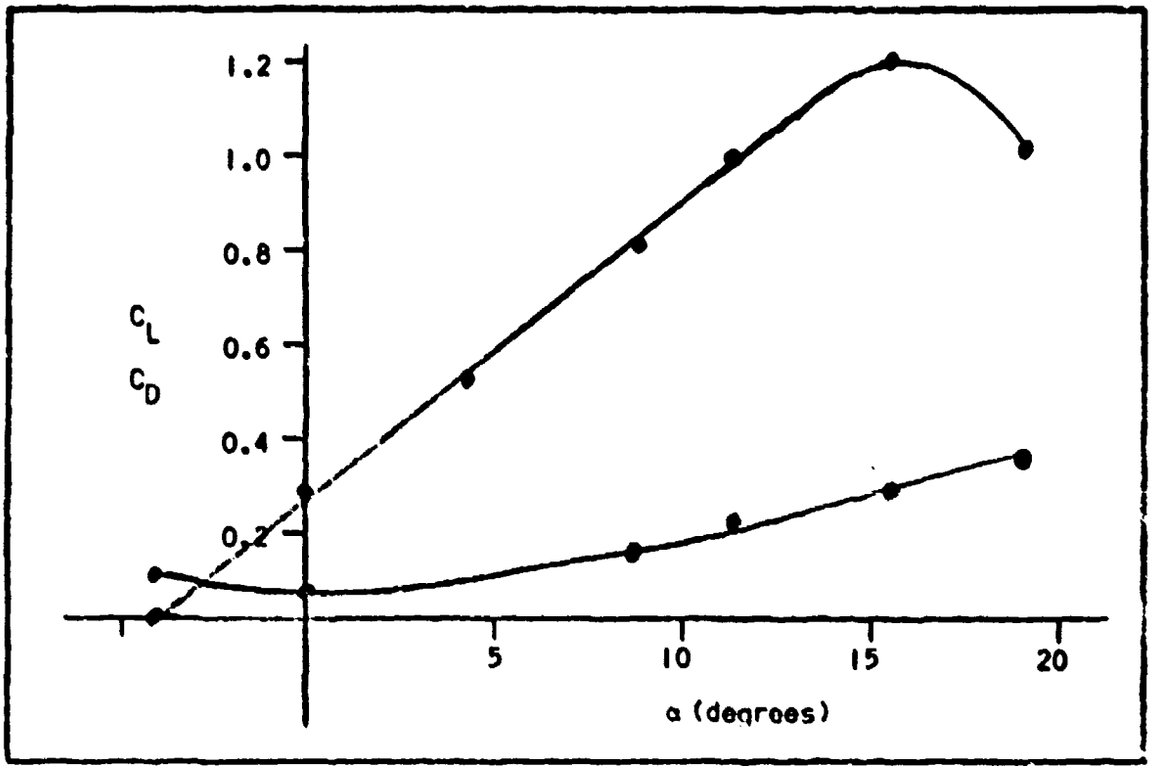

Fig. 13 Wing-Body-Tail Lift and Drag Curves

The airflow tests in this case were accomplished through the use of a bubble generator which dispersed neutrally bouyant bubbles into the airstream. This method allowed better evaluation of the airflow around the tail than was possible with tufting. The flow around the body was expected to be very similar to that around the body of the wing-body vehicle since the bodies were identical, and thus would not have to be studied as

carefully as tufting would have allowed. The flow around the tail was of major interest since any tail blockage within the normal angle of attack range would have introduced some type of instability into the model dynamics and would also have invalidated the analytical model in the affected range. The resulting streamlines showed no tail blockage at any angle of attack from -10° to +20°.

In this case as in the tailless case only the short period mode and the directional stability could be evaluated using the one degree of freedom mounts. In both cases, the modes were very stable and well damped.

Flight Tests

The flights, conducted in the same manner as the wing-body tests, resulted in demonstrating that the model was stable in all modes. The major problem that appeared could have been either slow damping of the launch perturbations from the helicopter rotor wash, or a weakly damped dutch roll mode with large amplitude convergent oscillations that resembled an exaggerated dutch roll oscillation. This problem could not be further evaluated in the flight test program since the vehicles were not of sufficient size to see at an altitude that would allow flight durations of sufficient length to see these perturbations damp out. Although this design did meet all of the design criteria, certain problems still existed that a further iteration of the design process would solve.

Design Iteration

Three major problems needed to be solved if the design was to be very successful: 1) the tail packaging problem needed a better solution so that the trade-off between packaging and stability would not be as great, 2) the tail flexibility problem had to be eliminated so that less

limitation on payload center of gravity location was necessary, and 3) the oscillations in the dutch roll mode as predicted by the analytical model and seen in the flight tests needed to be reduced. The first two problems could be reduced or eliminated by a different tail folding mechanism, and the dutch roll mode could be increased by an increase in the vertical tail effectiveness as shown in the sensitivity analysis. The tail modification presented in figure 14 was developed to solve all of the problems.

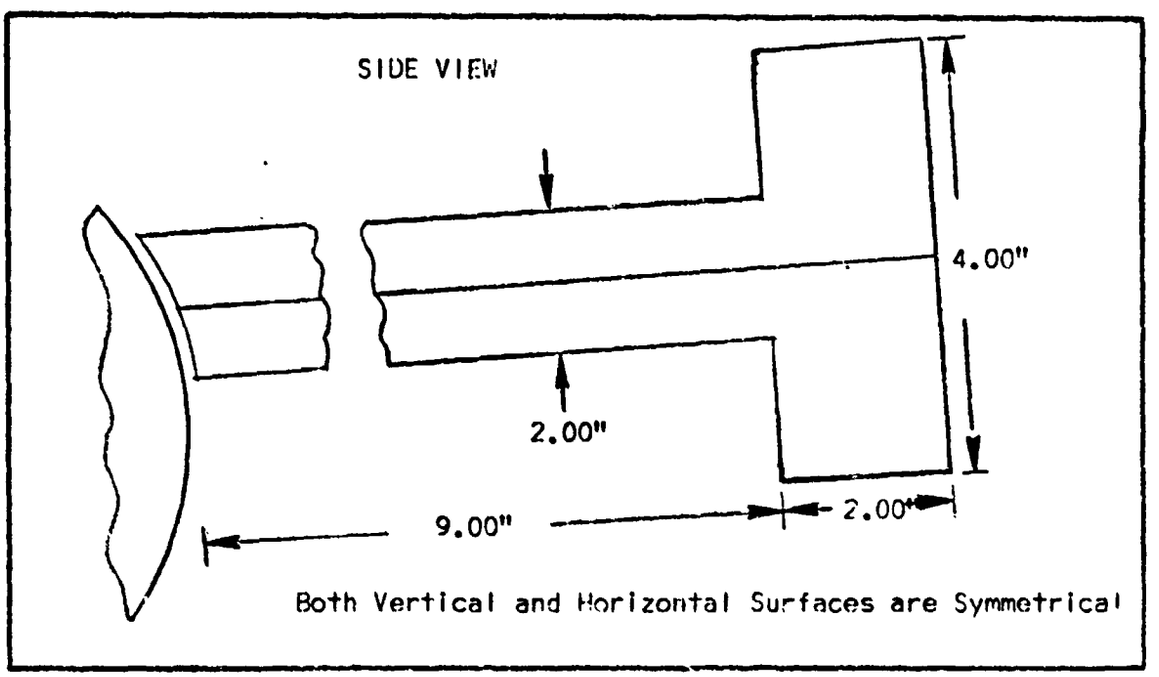

Fig. 14 Cruciform Tail Design

The resulting tail-boom was designed so that the vertical surface folded flat against the horizontal surface and the flat surface formed then wrapped around the circumference of the body. When unfolded, the vertical and horizontal surfaces formed a symmetrical cross that was rigid in the horizontal and vertical planes, thus eliminating the flexibility problem.

Although torsional rigidity was reduced with this form, the elastic axis of the tail-boom extended through the axis of symmetry of both the horizontal and vertical surfaces thus creating a symmetrical load distribution in symmetrical flight. Asymmetrical loadings could not be analyzed using the available model and therefore pending wind tunnel analysis were assumed negligible. The response of the resulting modification using the dimensions illustrated in figure 14 was:

Longitudinal:	Short Period		Phugoid	
	-3.9622×10^{-3}	$\pm\ 2.0363\times10^{-2}\ i$	-5.5374×10^{-5}	$7.8522\times10^{-4}\ i$
$\hat{V}$:	-2.0747×10^{-4}	$\pm\ 3.5663\times10^{-3}\ i$	2.5306×10^{-1}	$5.2263\times10^{-1}\ i$
α:	2.8357×10^{-1}	$\pm\ 6.5245\times10^{-1}\ i$	-3.6446×10^{-3}	$4.3088\times10^{-3}\ i$
$\hat{q}$:	-1.3605×10^{-2}	$\pm\ 5.2340\times10^{-3}\ i$	3.0338×10^{-4}	$5.6603\times10^{-4}\ i$
θ:	3.7237×10^{-1}	$5.9558\times10^{-1}\ i$	-7.0412×10^{-1}	$3.2994\times10^{-1}\ i$

Lateral:	Dutch Roll		Rolling Mode	Spiral
	-1.1909×10^{-3}	$1.2965\times10^{-2}\ i$	-2.2526×10^{-2}	-2.8964×10^{-4}
β:	1.1339×10^{-2}	$7.1615\times10^{-1}\ i$	2.0282×10^{-3}	-6.6366×10^{-3}
$\hat{p}$:	-4.3672×10^{-3}	$6.2010\times10^{-3}\ i$	-1.1620×10^{-2}	1.3168×10^{-3}
$\hat{r}$:	4.8779×10^{-2}	$3.6520\times10^{-3}\ i$	2.9664×10^{-3}	-2.9440×10^{-3}
ϕ:	-3.1064×10^{-2}	$6.9405\times10^{-1}\ i$	9.9993×10^{-1}	-9.9997×10^{-1}

In this analysis the inertial properties were assumed duplicated in the modified vehicle due to lack of sensitivity to inertia variation demonstrated in the sensitivity analysis. As seen in the root locus for these modes the response is significantly improved over the baseline vehicle. Figure 15 illustrates the root locus for each oscillatory mode.

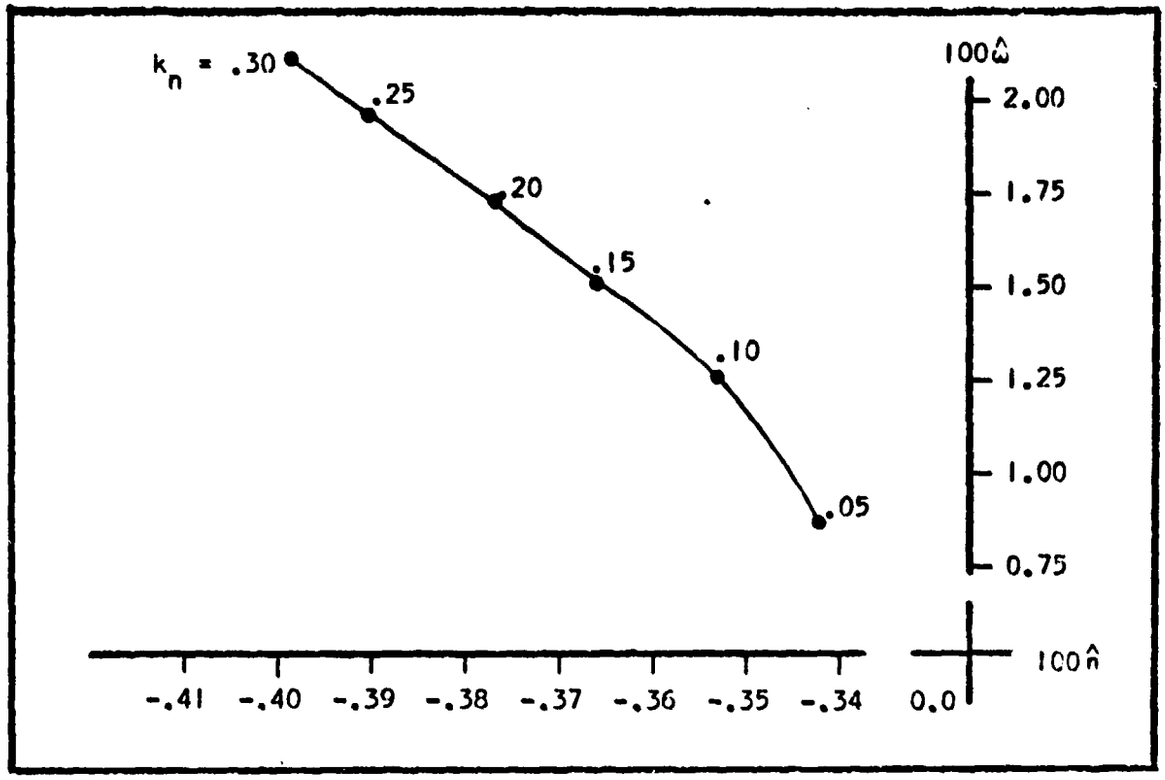

Fig. 15a Root Locus for Cruciform Tail - Short Period

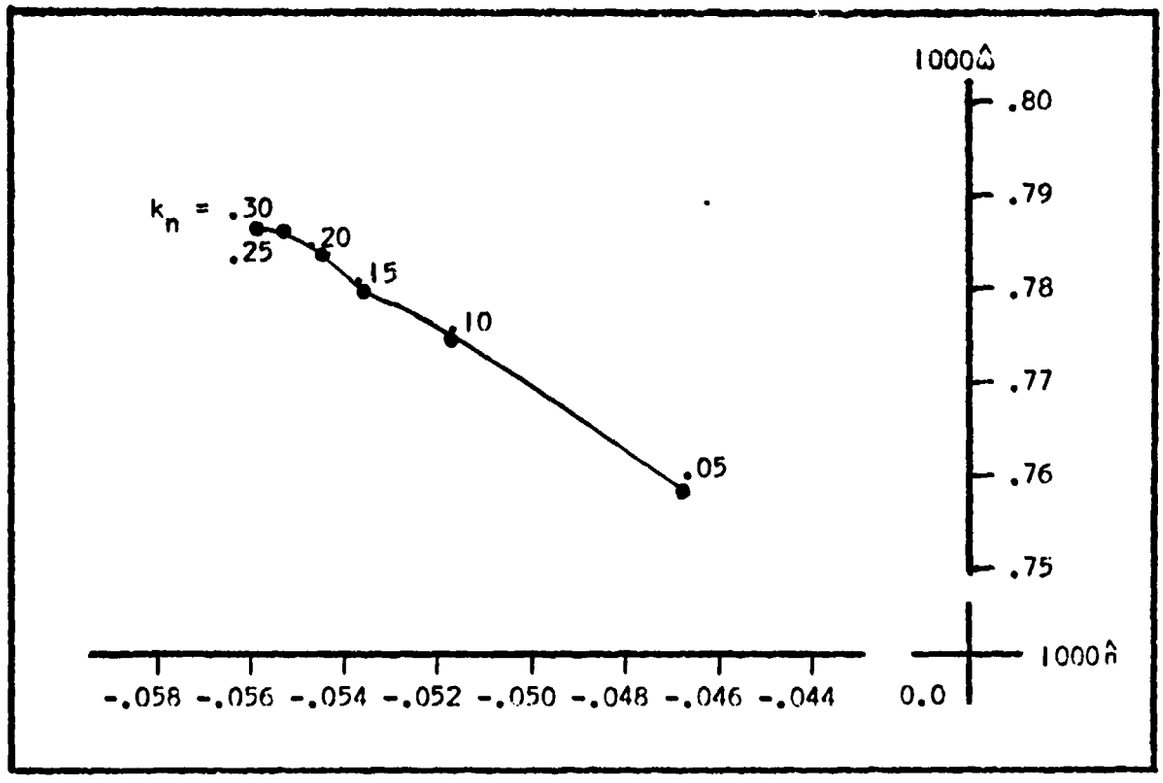

Fig. 15b Root Locus for Cruciform Tail - Phugoid

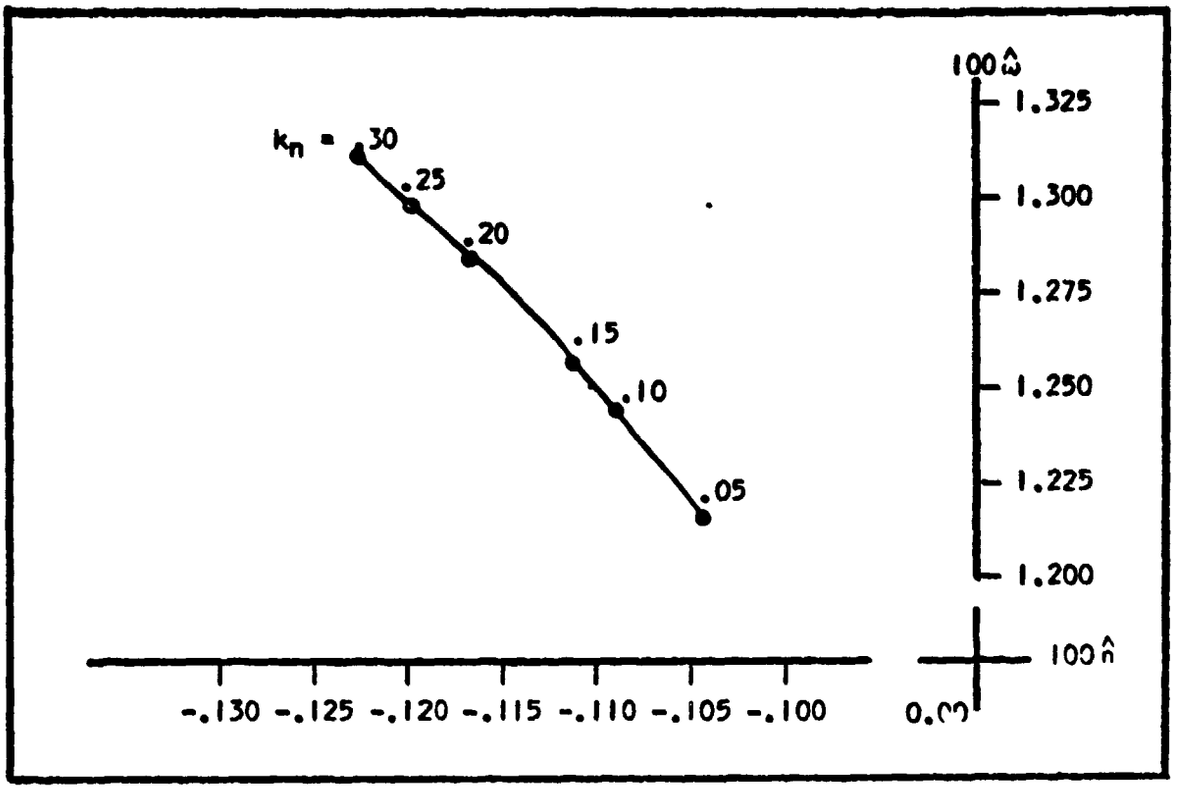

Fig. 15c Root Locus for Cruciform Tail - Dutch Roll

Wind Tunnel Tests

All of the wind tunnel tests run on the other two configurations were repeated for this modified version. The only significant difference from the results already discussed for the baseline tailed vehicle were the lift and drag curves presented in figure 16. It should be noted that the glide ratio improved greatly over the baseline vehicle. This improvement was due to the reduction in base drag which was a result of the new tail-boom aerodynamically fairing in the body so that aerodynamically it seemed longer than it was really.

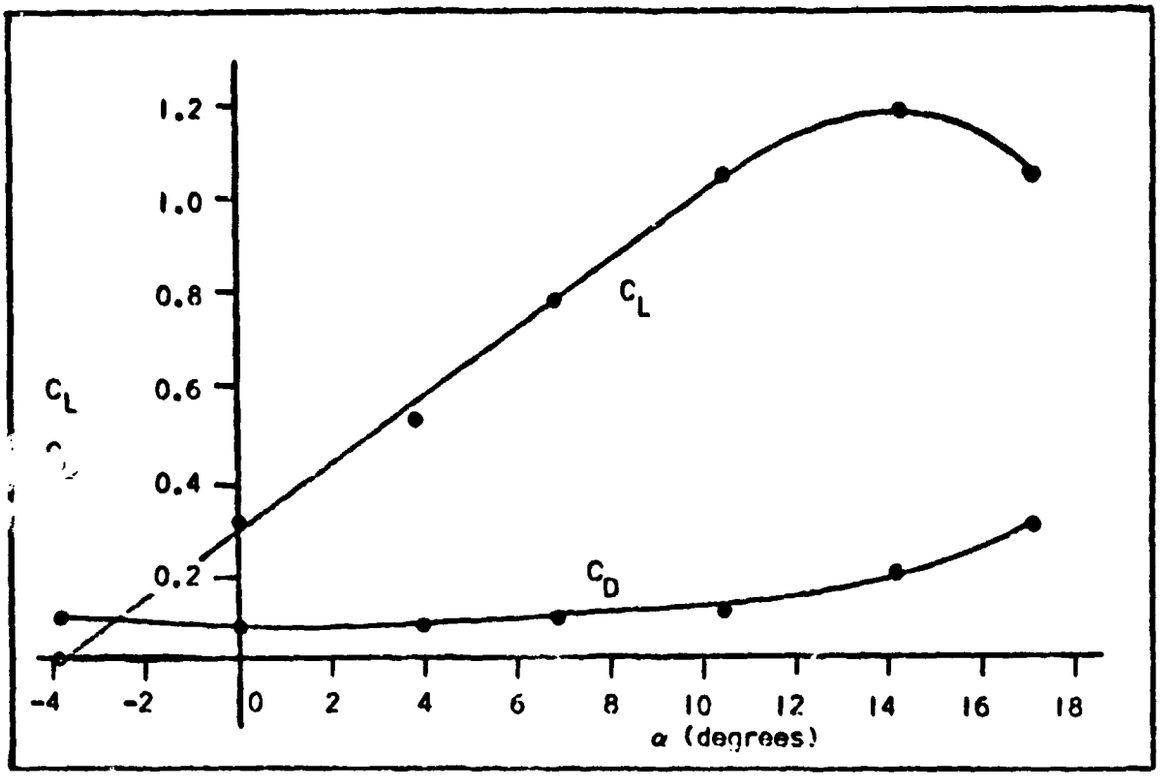

Fig. 16 Cruciform Tail Lift and Drag Curves

Flight Test Analysis

No aircraft support was available to provide an airborne platform to launch the vehicle from, so this set of flight tests had to be hand-launched from the top of a building. Since there was no similarity in the post-launch disturbances between this vehicle and the previous vehicles, direct comparison was impossible. Even so, it was easily observed that this vehicle was more stable than the other vehicles tested and thus the design was partially proven by this set of tests.

Iteration Conclusions

As a result of this limited set of tests and the other data on the configuration, it was decided that this vehicle was a satisfactory design

to submit to the Avionics Laboratory. The next step in the analytic procedure was to evaluate the final vehicle's performance.

Performance Analysis

In order to evaluate the performance of the vehicle without arbitrarily fitting the drag to a parabolic polar, the method of reference 12 was used in the performance analysis. It was shown in this reference that it was possible to evaluate the coefficient of lift and thus the angle of attack for both maximum endurance and maximum range from a graph of C_L vs. C_D in the first instance and $C_L^{3/2}$ vs. C_D in the second instance. The two curves are shown in figure 17a and 17b.

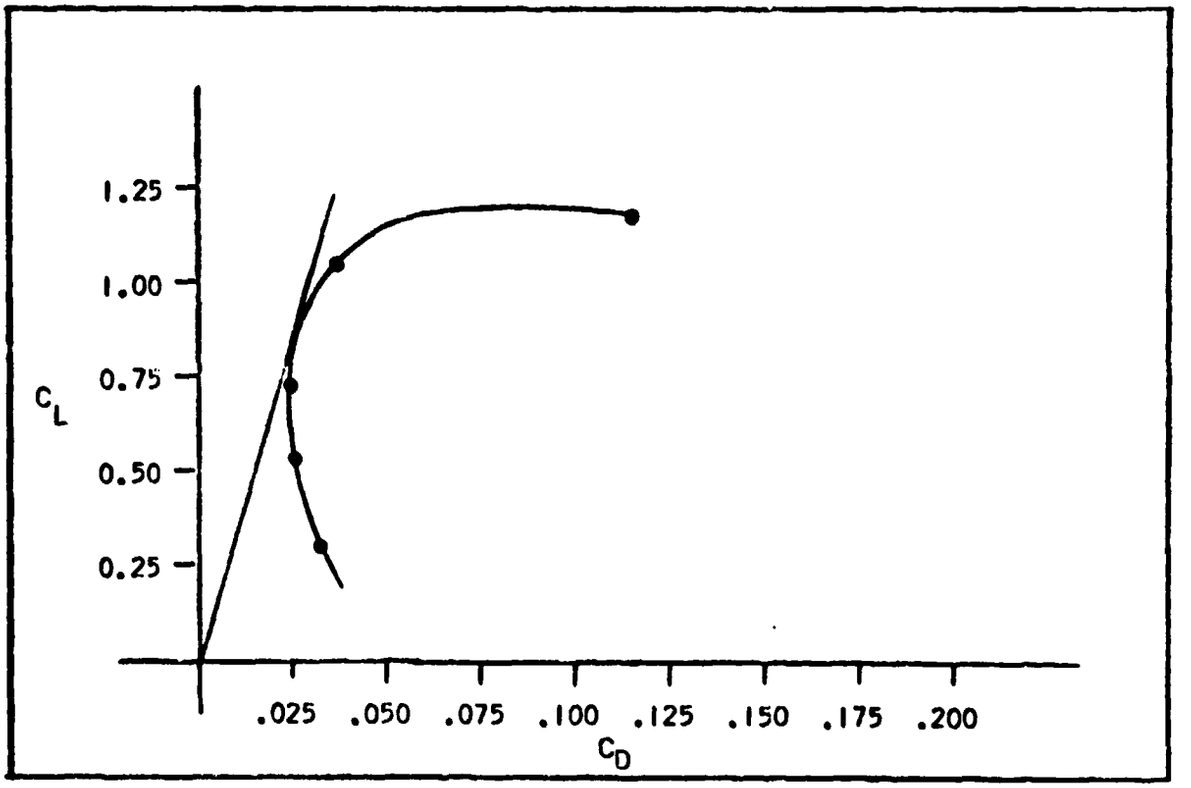

Fig. 17a Maximum Range Calculation

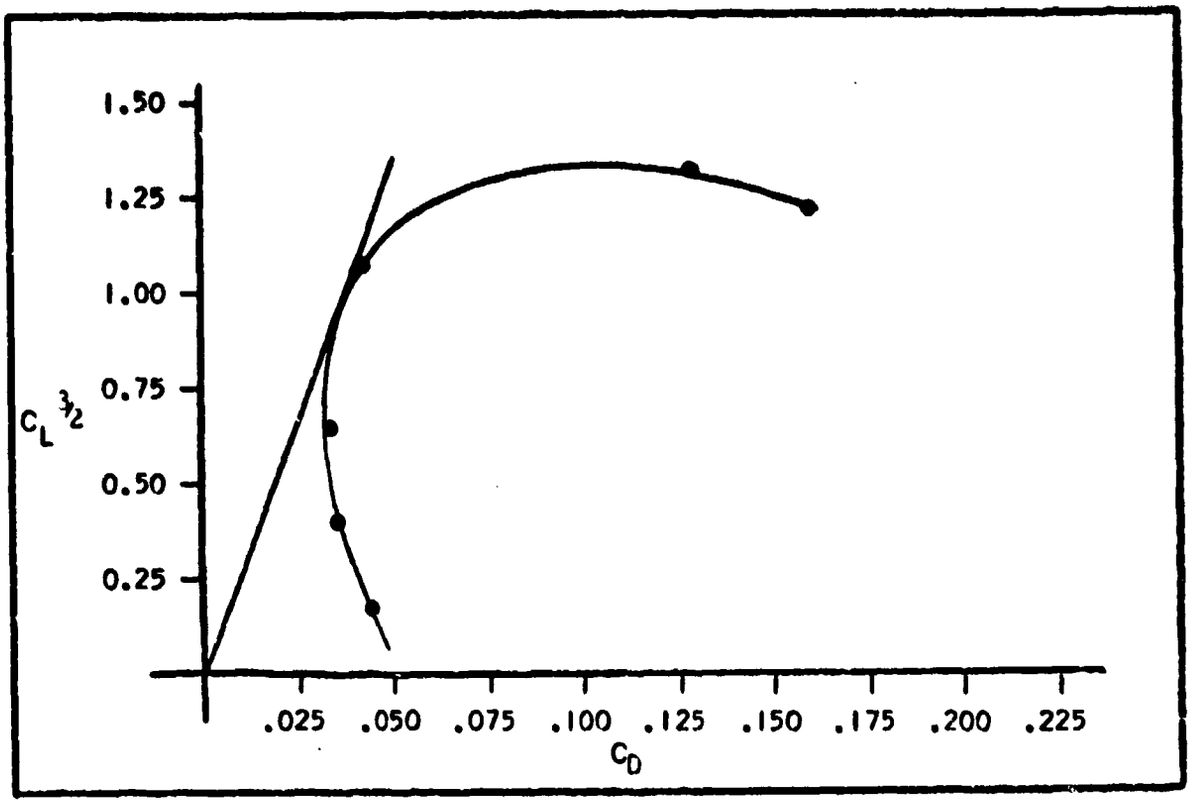

Fig. 17b Maximum Endurance Calculation

As presented in the reference, the point of maximum range occurs at the point on the C_L vs. C_D curve where a line drawn from the origin is tangent to the curve. In a similar fashion, the point of maximum endurance is found on the second curve. The performance points are:

Maximum Range: $C_L = .8500$

$= 8.5°$

Maximum Endurance: $C_L = 1.0000$

$= 10.5°$

One further factor had to be taken into account before the trim angle of attack could be set. At speeds below the speed for L/D_{max}

an aircraft is unstable and any disturbance will cause the vehicle to decrease speed and to eventually stall, therefore the trim angle of attack had to be a compromise between speed stability and maximum range. Since the exact function of the payload will probably vary during any production life of the vehicle, a trim angle of 7° was chosen to represent a solution close to both the optimum angles for best range and best endurance and was still a speed stable angle of attack.

V. CONCLUSIONS AND RECOMMENDATIONS

Conclusions

The major conclusion arrived at from the analysis was that the cruciform tail design was the best design to submit to the Air Force Avionics Laboratory in response to their design request. The design meets all of the packaging requirements and exceeds all of the performance requirements by a significant margin.

A secondary conclusion was that tailless vehicles as a class should be excluded from further consideration as a possible configuration to meet the desired design requirements. This class of vehicles has major stability problems and at least in the above analysis, no possible solutions to these problems were available. It appeared that if the launch dynamics of this class of vehicles were considered, the stability problem would be insolvable.

Recommendations

It is recommended that further analysis of the proposed vehicle be conducted into the areas excluded from the above analysis. In particular, the launch dynamics need to be carefully studied because it is possible that the perturbations from the launch would cause the vehicle to stabilize into some undesirable flight condition. To study this area, an extensive set of wind tunnel tests needs to be conducted to determine the vehicle dynamic stability derivatives so that a six degree of freedom non-linear analysis can be conducted. Finally flight tests of the vehicle on a fully instrumented test range under simulated operational conditions need to be conducted.

Bibliography

1. Jones, R.T., Notes on the Stability and Control of Tailless Airplanes. NACA Technical Note 857, Washington: National Advisory Committee for Aeronautics, 1946.

2. Hoerner, S.F., Fluid-Dynamic Drag. New Jersey: S.F. Hoerner, 1958.

3. Ellison, D.E. and Malthan, L.V., USAF Stability and Control Methods. U.S.A.F. Flight Control Division, Flight Dynamics Laboratory, WPAFB, Ohio, July 1963.

4. Etkin, Bernard. Dynamics of Atmospheric Flight. New York: John Wiley & Sons, Inc., 1972

5. Abbott, I.H. and Von Doenhoff, A.E., Theory of Wing Sections. New York: Dover Publications, Inc., 1959

6. Bisplinghoff, R.L., Ashley, H., and Half, R.L., Aeroelasticity. Reading, Mass.: Addison-Wesley Publishing Company, Inc., 1955

7. Toll, T.A. and Queijo, M.J., Approximate Relations and Charts for Low-Speed Stability Derivatives of Swept Wings. NACA Technical Note 1581. Washington: National Advisory Committee for Aeronautics, May 1948.

8. Roskam, J., Methods for Estimating Stability and Control Derivatives of Conventional Subsonic Airplanes. by Author: 519 Boulder, Lawerence Kansas, 1971.

9. Blakelock, J.H., Automatic Control of Aircraft and Missiles. New York: John Wiley & Sons, Inc., 1965.

10. Dennis, D.R., The Unpowered, Free Flight Aircraft Model. RAE Technical Note No. Aero. 2881, London: Royal Aircraft Establishment, March 1963.

11. Burk, S.M., Wind-Tunnel Investigation of Aerodynamic Characteristics of a Rigid-Wing Recovery System. NASA Technical Note D-5922, Washington: National Aeronautics and Space Administration, August 1970.

12. Miele, A., Flight Mechanics: Theory of Flight Paths. Reading, Mass: Addison-Wesley Publishing Company, Inc., 1962.

In the appendices that follow the longitudinal data is normalized with $\theta = 1.0$, nd the lateral data is normalized with $\phi = 1.0$. The dashed vectors indicate a magnitude too small to be visible.

Appendix A

Longitudinal Response Data For The Wing-Body Configuration

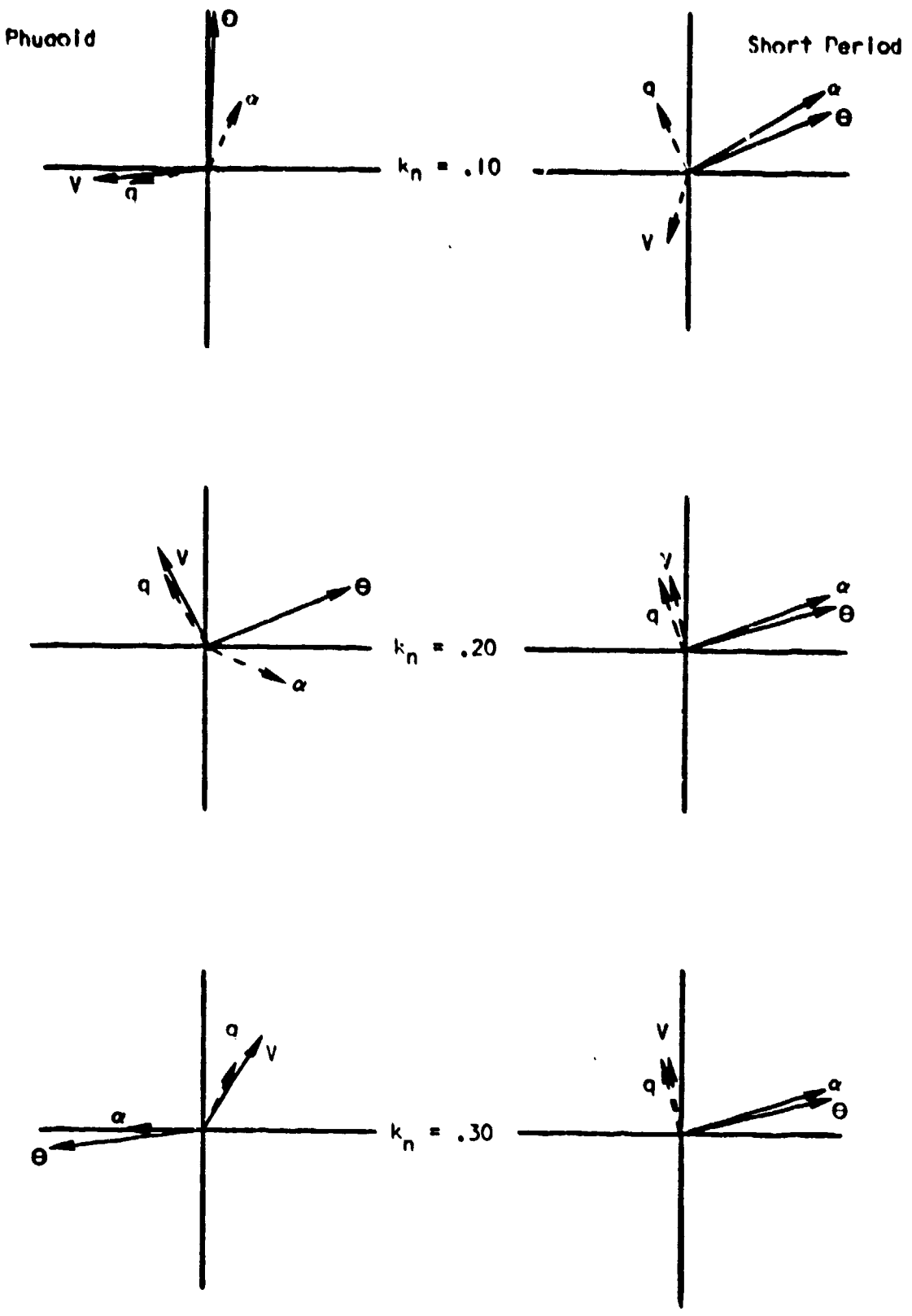

Appendix H

Lateral Response Data For The Wing-Body Configuration

Dutch Roll Mode

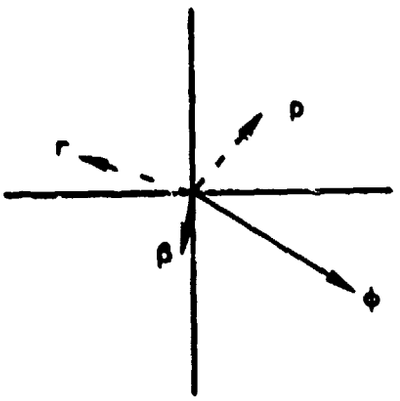

$k_n = .10$

Rolling Mode

$\beta:\phi:\psi = -.1529:1:.1215$
$\beta:p:r = 1:.6160:.0730$

Spiral Mode

$\beta:\phi:\psi = .0062:1:-4.4730$
$\beta:p:r = 1:-.0409:.4728$

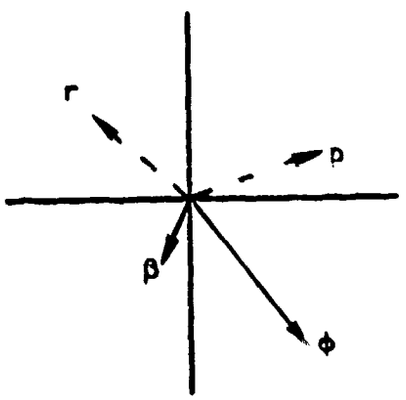

$k_n = .20$

Rolling Mode

$\beta:\phi:\psi = -.1995:1:.1701$
$\beta:p:r = 1:.5040:.0830$

Spiral Mode

$\beta:\phi:\psi = .0060:1:-4.9176$
$\beta:p:r = 1:-.0321:.4847$

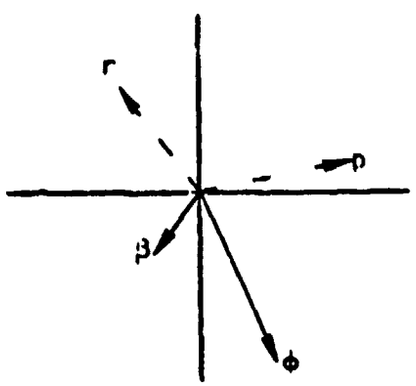

$k_n = .30$

Rolling Mode

$\beta:\phi:\psi = -.2507:1:.2230$
$\beta:p:r = 1:.4263:.0914$

Spiral Mode

$\beta:\phi:\psi = .0059:1:-5.2871$
$\beta:p:r = 1:-.0255:.4928$

Appendix C

Longitudinal Response Data For The Wing-Body-Tail Configuration

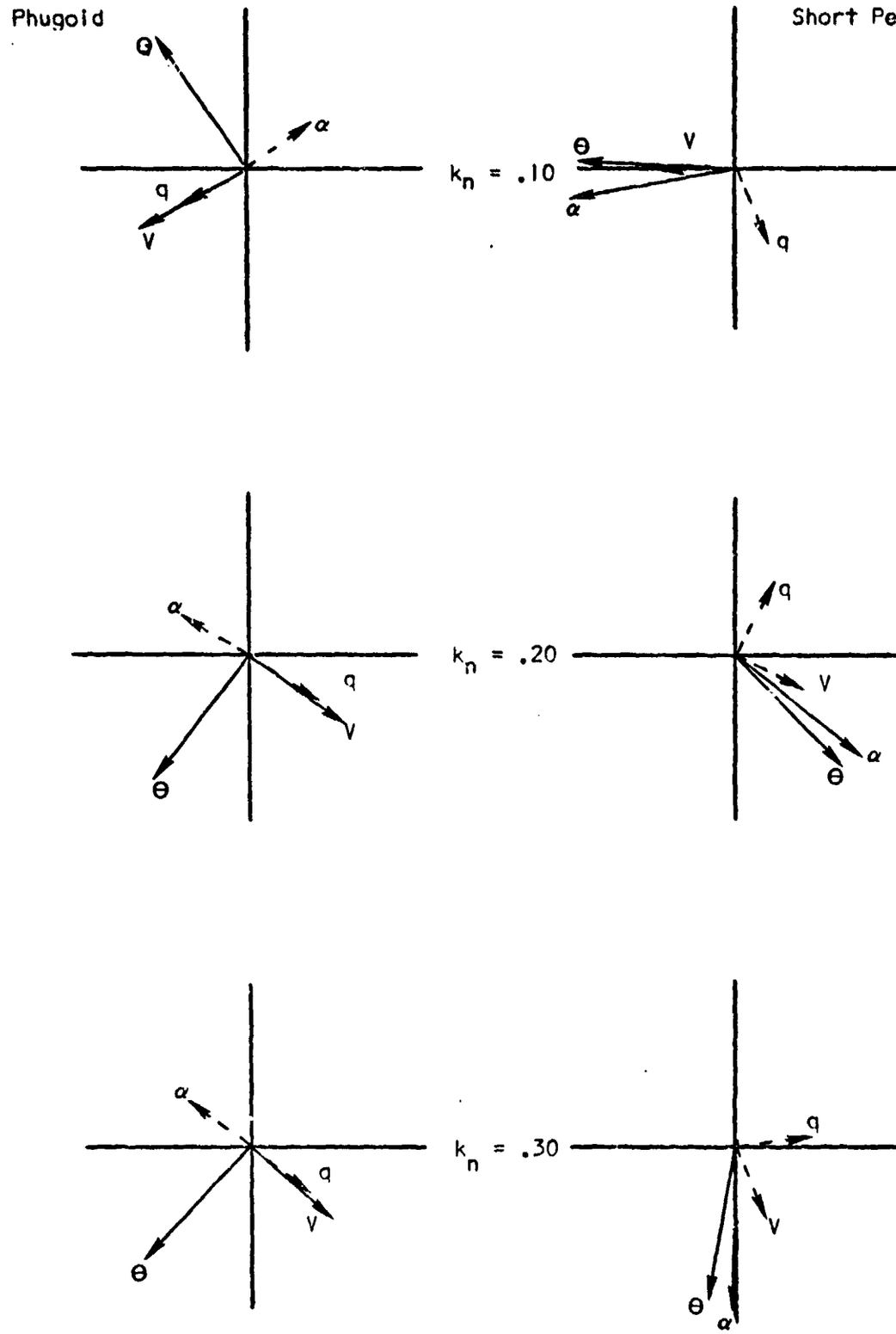

Appendix D

Longitudinal Derivative Sensitivity Analysis

Derivative:	Short Period:		Phugoid:	
C_{L_α} + 20%	-6.3524×10^{-3}	2.0841×10^{-2} i	-5.4882×10^{-5}	7.7821×10^{-4} i
C_{L_α} - 20%	-6.5644×10^{-3}	2.1948×10^{-2} i	-5.5868×10^{-5}	7.8223×10^{-4} i
$C_{L_{\dot\alpha}}$ + 50%	-6.7840×10^{-3}	2.1189×10^{-2} i	-5.5222×10^{-5}	7.7737×10^{-4} i
$C_{L_{\dot\alpha}}$ - 50%	-6.7888×10^{-3}	2.1207×10^{-2} i	-5.5230×10^{-5}	7.7737×10^{-4} i
C_{L_q} + 20%	-6.7868×10^{-3}	2.1200×10^{-2} i	-5.5224×10^{-5}	7.7728×10^{-4} i
C_{L_q} - 20%	-6.7897×10^{-3}	2.1222×10^{-2} i	-5.5204×10^{-5}	7.7651×10^{-4} i
C_{M_q} + 20%	-7.5869×10^{-3}	2.1042×10^{-2} i	-5.5056×10^{-5}	7.7351×10^{-4} i
C_{M_q} - 20%	-6.0424×10^{-3}	2.1314×10^{-2} i	-5.5403×10^{-5}	7.8101×10^{-4} i
$\hat{I}_{yy}$ + 10%	-6.3191×10^{-3}	2.0280×10^{-2} i	-5.5042×10^{-5}	7.7739×10^{-4} i
$\hat{I}_{yy}$ - 10%	-7.3830×10^{-3}	2.2300×10^{-2} i	-5.5416×10^{-5}	7.7735×10^{-4} i

Appendix E

Lateral Response Data for the Wing-Body-Tail Configuration

Dutch Roll Mode

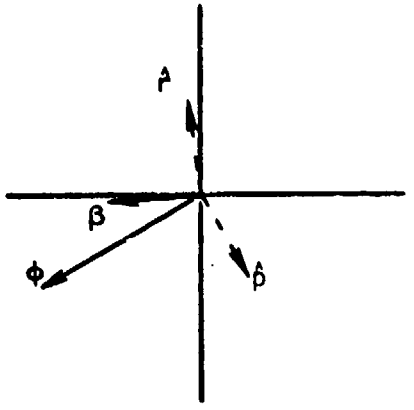

$k_n = .10$

Rolling Mode

$\beta:\phi:\psi = -.0695:1:-.0568$
$\beta:p:r = 1:.3370:-.0190$

Spiral Mode

$\beta:\phi:\psi = .0089:1:-2.2869$
$\beta:p:r = 1:-.1236:.3321$

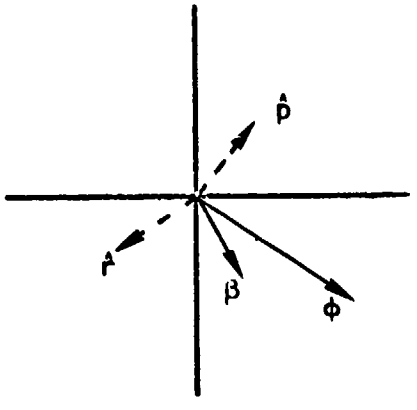

$k_n = .20$

Rolling Mode

$\beta:\phi:\psi = -.0674:1:-.0592$
$\beta:p:r = 1:.3468:-.0204$

Spiral Mode

$\beta:\phi:\psi = .0090:1:-2.1249$
$\beta:p:r = 1:-.1342:.3305$

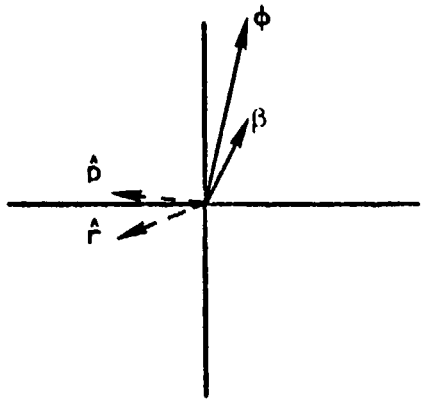

$k_n = .30$

Rolling Mode

$\beta:\phi:\psi = -.0654:1:-.0615$
$\beta:p:r = 1:.3565:-.0218$

Spiral Mode

$\beta:\phi:\psi = .0090:1:-1.9798$
$\beta:p:r = 1:-.1450:.3290$

Appendix F

Lateral Derivative Sensitivity Analysis

Derivative:	Dutch Roll Mode	Rolling Mode	Spiral Mode
C_{y_β} + 50%	$4.0279\times10^{-4} \pm 8.1171\times10^{-3}i$	-4.4651×10^{-3}	-2.7794×10^{-4}
C_{y_β} - 50%	$4.1536\times10^{-4} \pm 8.1174\times10^{-3}i$	-4.4628×10^{-3}	-2.7803×10^{-4}
C_{y_p} + 50%	$4.0896\times10^{-4} \pm 8.1172\times10^{-3}i$	-4.4637×10^{-3}	-2.7798×10^{-4}
C_{y_p} - 50%	$4.0919\times10^{-4} \pm 8.1169\times10^{-3}i$	-4.4642×10^{-3}	-2.7799×10^{-4}
C_{y_r} + 50%	$4.0928\times10^{-4} \pm 8.1145\times10^{-3}i$	-4.4642×10^{-3}	-2.7815×10^{-4}
C_{y_r} - 50%	$4.0886\times10^{-4} \pm 8.1198\times10^{-3}i$	-4.4637×10^{-3}	-2.7782×10^{-4}
C_{l_β} + 50%	$-1.3113\times10^{-4} \pm 7.8780\times10^{-3}i$	-3.5570×10^{-3}	-1.0452×10^{-4}
C_{l_β} - 50%	$4.0907\times10^{-4} + 8.1172\times10^{-3}i$	-4.4639×10^{-3}	-2.7798×10^{-4}
C_{l_p} + 50%	$3.0351\times10^{-4} + 8.1895\times10^{-3}i$	-5.3427×10^{-3}	-2.3512×10^{-4}
C_{l_p} - 50%	$5.2562\times10^{-4} \pm 8.0038\times10^{-3}i$	-3.4235×10^{-3}	-3.5983×10^{-4}
C_{l_r} + 50%	$3.8813\times10^{-4} \pm 8.1506\times10^{-3}i$	-4.4951×10^{-3}	-2.0494×10^{-4}
C_{l_r} - 50%	$4.3047\times10^{-4} \pm 8.0838\times10^{-3}i$	-4.4314×10^{-3}	-3.5331×10^{-4}
C_{n_β} + 50%	$1.0107\times10^{-4} \pm 9.6416\times10^{-3}i$	-3.9515×10^{-3}	-1.7438×10^{-4}
C_{n_β} - 50%	$9.3036\times10^{-4} \pm 6.4461\times10^{-3}i$	-5.3439×10^{-3}	-4.4060×10^{-4}
C_{n_p} + 50%	$1.4695\times10^{-4} \pm 7.9325\times10^{-3}i$	-3.8904×10^{-3}	-3.2724×10^{-4}
C_{n_p} - 50%	$6.4104\times10^{-4} \pm 8.3012\times10^{-3}i$	-4.9622×10^{-3}	-2.4362×10^{-4}
C_{n_r} + 50%	$1.0094\times10^{-4} \pm 8.0028\times10^{-3}i$	-4.3872×10^{-3}	-4.9462×10^{-4}
C_{n_r} - 50%	$7.2023\times10^{-4} \pm 8.2064\times10^{-3}i$	-4.5265×10^{-3}	-8.1076×10^{-5}

Inertia:	Dutch Roll Mode	Rolling Mode	Spiral Mode
I_{xx} + 10%	$3.4818\times10^{-4} \pm 8.0523\times10^{-3}i$	-4.1427×10^{-3}	-2.9727×10^{-4}
I_{xx} - 10%	$4.7466\times10^{-4} \pm 8.1952\times10^{-3}i$	-4.6341×10^{-3}	-2.7673×10^{-4}
I_{zz} + 10%	$4.9026\times10^{-4} \pm 7.8165\times10^{-3}i$	-4.5011×10^{-3}	-2.7094×10^{-4}
I_{zz} - 10%	$3.1217\times10^{-4} \pm 8.4681\times10^{-3}i$	-4.4230×10^{-3}	-2.8544×10^{-4}

Appendix G

Lateral Response for Modified Wing-Body-Tail Configuration

Dutch Roll Mode

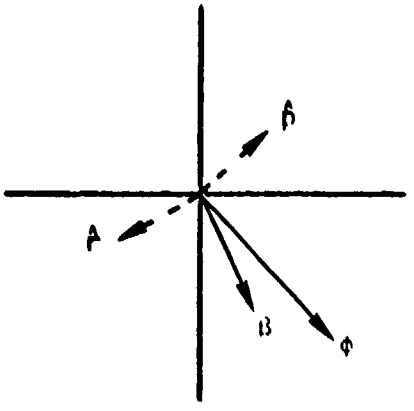

$k_n = .10$

Rolling Mode

$\beta:\phi:\psi = -.0552:1:-.0946$
$\beta:\hat{p}:\hat{r} = 1:.3738:-.0353$

Spiral Mode

$\beta:\phi:\psi = .0106:1:-2.2418$
$\beta:\hat{p}:\hat{r} = 1:-.1061:.2783$

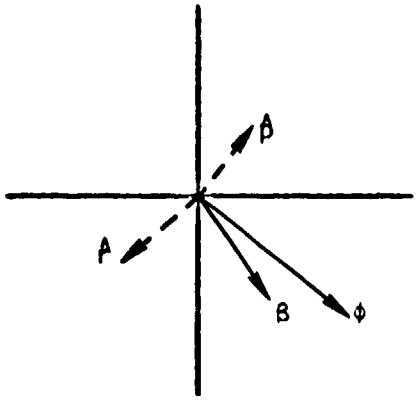

$k_n = .20$

Rolling Mode

$\beta:\phi:\psi = -.0478:1:-.0999$
$\beta:\hat{p}:\hat{r} = 1:.4236:-.0422$

Spiral Mode

$\beta:\phi:\psi = .0109:1:-2.1634$
$\beta:\hat{p}:\hat{r} = 1:-.1080:.2718$

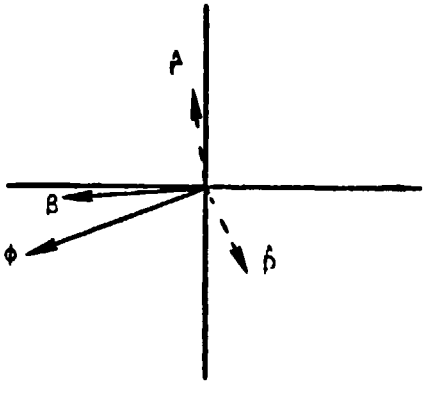

$k_n = .30$

Rolling Mode

$\beta:\phi:\psi = -.0452:1:-.1051$
$\beta:p:r = 1:.4410:-.0462$

Spiral Mode

$\beta:\phi:\psi = .0111:1:-2.0912$
$\beta:\hat{p}:\hat{r} = 1:-.1098:.2656$

Appendix H

Longitudinal Response Data for the Cruciform Tail Configuration

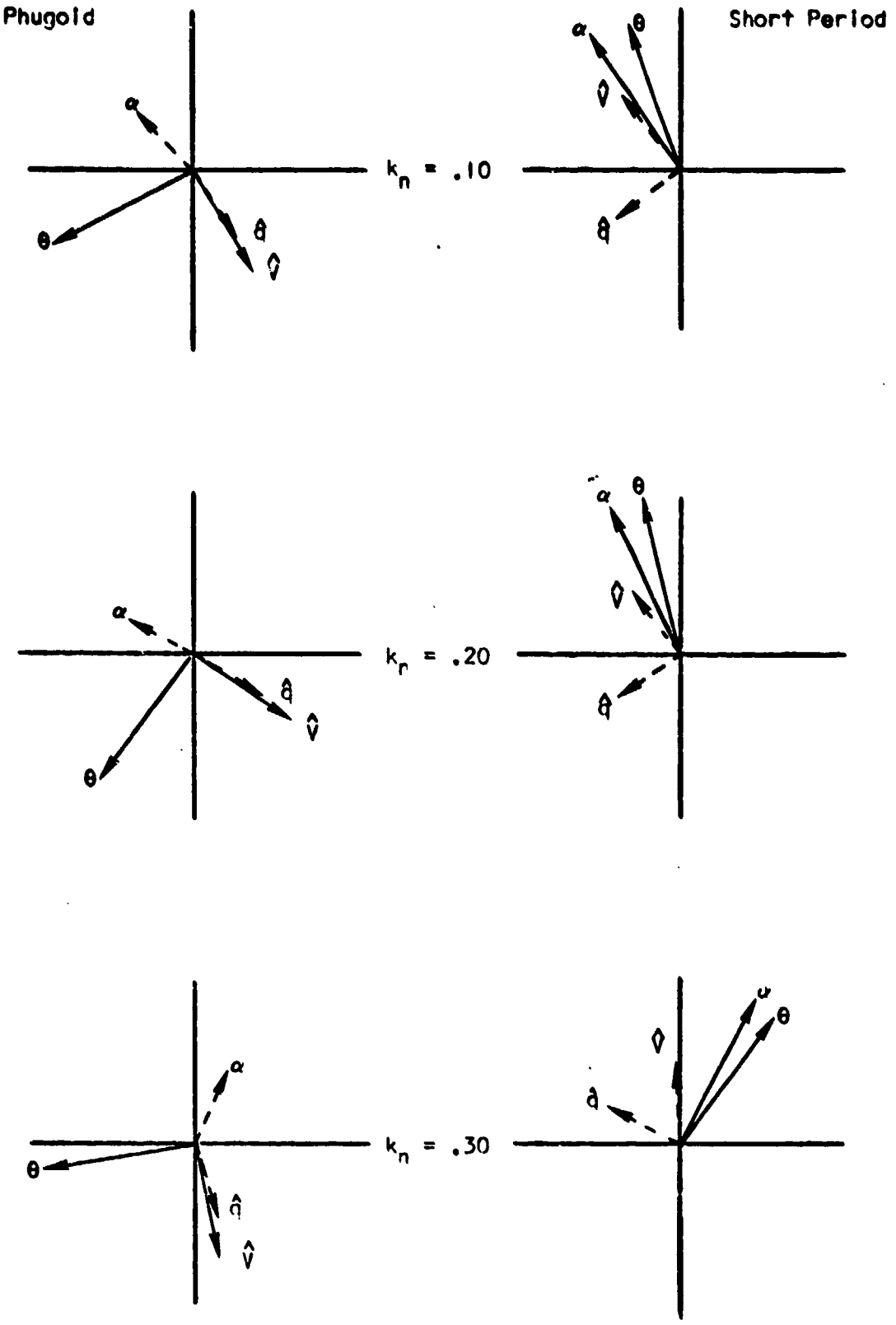

Appendix I

Lateral Response Data for the Cruciform Tail Configuration

Dutch Roll Mode

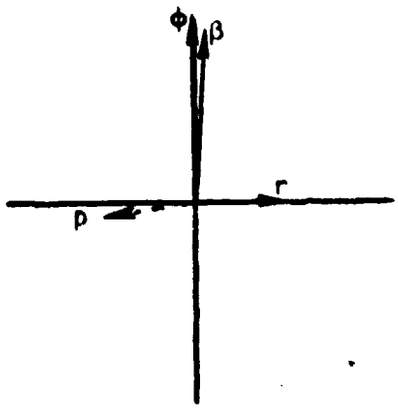

$k_n = .10$

Rolling Mode

$\beta:\phi:\psi = .0018:1:-.2512$
$\beta:p:r = 1:-6.3512:1.6080$

Spiral Mode

$\beta:\phi:\psi = .0066:1:-2.0008$
$\beta:p:r = 1:-.1949:.4477$

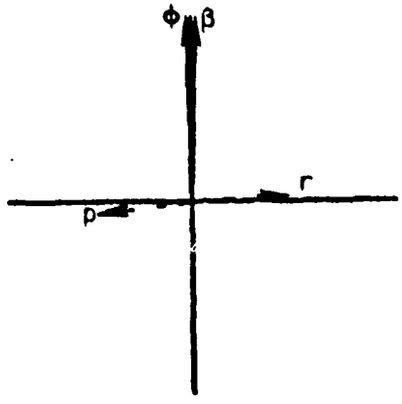

$k_n = .20$

Rolling Mode

$\beta:\phi:\psi = .0020:1:-.2526$
$\beta:p:r = 1:-5.9322:1.5105$

Spiral Mode

$\beta:\phi:\psi = .0066:1:-1.9629$
$\beta:p:r = 1:-.1988:.4465$

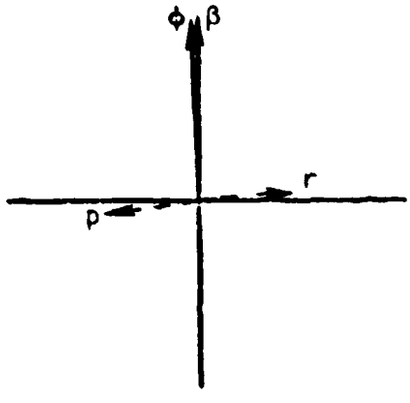

$k_n = .30$

Rolling Mode

$\beta:\phi:\psi = .0021:1:-.2541$
$\beta:p:r = 1:-5.5077:1.4106$

Spiral Mode

$\beta:\phi:\psi = .0067:1:-1.9153$
$\beta:p:r = 1:-.2014:.4397$

Vita: Phillip L. Abold

Phillip L. Abold was born on May 23, 1946 in Baldwinsville, New York. After an uneventful childhood, he graduated from Baker High School in Baldwinsville, New York. Graduation from high school was followed by four years at the U.S. Air Force Academy from which he graduated in 1968 with a Bachelor of Science in Aeronautical Engineering, and a commission as a Second Lieutenant in the United States Air Force. Pilot training at Randolph Air Force Base, Texas was sucessfully completed in 1969 and a year in S.E. Asia followed as a Forward Air Controller. After the S.E. Asia tour came two years as an instructer pilot at Laughlin AFB, Texas. In 1973 he was selected for admission to the Air Force Institute of Technology which he entered in June of that year. He graduated with a Master of Science in Aeronautical Engineering, specializing in aircraft stability and control in December 1974.